Optical Fiber Sensor Technologies for Efficient and Economical Oil Recovery

Annual Report

Reporting Period Start Date: 1 Oct 98
Reporting Period End Date: 31 Sept 99

Principal Authors: A. Wang, H. Xiao, R. May

Issue Date: 29 October 99

DOE Award Number: DE-FG26-988C15167

Submitted by: Photonics Laboratory
Bradley Department of Electrical and Computer Engineering
Virginia Tech
Blacksburg, VA 24061-0111

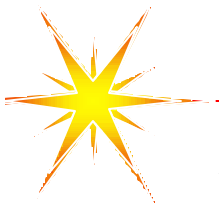

PHOTONICS
LABORATORY
Virginia Polytechnic Institute and State University

Disclaimer:

Abstract

Efficient and complete recovery of petroleum reserves from existing oil wells has proven difficult due to a lack of robust instrumentation that can monitor processes in the downhole environment. Commercially available sensors for measurement of pressure, temperature, and fluid flow exhibit shortened lifetimes in the harsh downhole conditions, which are characterized by high pressures (up to 20 kpsi), temperatures up to 250°C, and exposure to chemically reactive fluids. Development of robust sensors that deliver continuous, real-time data on reservoir performance and petroleum flow pathways will facilitate application of advanced recovery technologies, including horizontal and multi-lateral wells.

The main objective of the research program is to develop cost-effective, reliable fiber sensor instrumentation for real-time monitoring and /or control of various key parameters crucial to efficient and economical oil production. This report presents the detailed research work and technical progress from October 1, 1998 to September 30, 1999. The research performed over the first year of the program has followed the schedule as proposed, and solid research progress has been made in specification of the technical requirements, design and fabrication of the SCIIB sensor probes, development of the sensor systems, development of DSP-based signal processing techniques, and construction of the test systems. These technical achievements will significantly help to advance continued research on sensor tests and evaluation during the second year of the program.

Table of Contents

List of Figures

Executive Summary

This report summarizes technical progress over the first twelve months of the Optical Fiber Sensor Technologies for Efficient and Economical Oil Recovery program, funded by the Federal Energy Technology Center of the U.S. Department of Energy, and performed by the Photonics Laboratory of the Bradley Department of Electrical and Computer Engineering at Virginia Tech. The main objective for this three and one-half year program is the development and demonstration of cost-effective, reliable optical fiber sensors for the measurement of temperature, pressure, flow, and acoustic waves in downhole environments for use in oil recovery.

The sensors being developed under this program are based on the Self-Calibrated Interferometric/Intensity-Based (SCIIB) fiber optic sensor configuration invented at the Photonics Laboratory. The SCIIB design measures displacement (elongation or contraction) of a small Fabry-Perot interferometer cavity constructed in an optical fiber. The Fabry-Perot assembly is typically cylindrical, and generally has dimensions on the order of 0.1 mm in diameter and 5 mm long. By proper mechanical design of the assembly, physical parameters such as pressure, temperature, and flow can be made to induce a displacement in the Fabry-Perot assembly, which may then be measured by the SCIIB system. In the SCIIB design, the Fabry-Perot assembly is designed so that the output of the cavity over the sensor's dynamic range is limited to remain in the quasi-linear region of the interference signal output by the cavity. In this way, interpretation of the nonlinear output of typical interferometers is avoided, simplifying the signal processing.

The SCIIB system uses optical filtering to process the optical signal output by the Fabry-Perot cavity so that two signals are produced: one which contains information about the cavity displacement, and another that contains information regarding undesired effects in the first signal, such as fluctuations in the optical source power, or changes in optical fiber loss. The second signal is used as a reference to eliminate these undesired effects, and provide self-calibration functions in the sensor.

During the first twelve months of the program, the research included determination of requirements for the sensors, development of SCIIB signal processing facilities, development of a system for the automated fabrication of SCIIB sensors, the design and investigation of pressure, acoustic, and temperature sensors, and the acquisition of equipment for sensor testing. These accomplishments are summarized below.

- The requirements for sensors intended for instrumentation of downhole oil recovery processes were determined by consultation with engineers at Baker Hughes and Chevron Research and Technology company. These requirements include specifications for operating range, accuracy, resolution, and operating temperature ranges. These requirements were adopted as goals for the design of the sensors in the remainder of the program.

- The optoelectronic system for processing the optical output of the SCIIB sensors was designed, constructed, and tested. Two SCIIB systems were assembled: one optimized for use with single-mode optical fiber, and the other for use with multimode optical fiber. Single-mode fiber will typically be used for applications in which the SCIIB system will be located more than one kilometer from the sensor. The multimode system is intended for applications where the separation is less. The multimode SCIIB system was tested to evaluate the self-calibration function of the system, and the results indicated that the system provided excellent self-compensation for losses in the optical fiber induced by bending. Also, the effect of changes in the optical spectrum of the light which result when the fiber is bent was investigated. The results indicate that fiber that is specially designed to be insensitive to bends will perform better than standard telecommunications optical fiber.

- A prototype SCIIB sensor system which uses a digital signal processor (DSP) to implement high speed computation for measurement of acoustic and seismic signals was investigated. The system will utilize an amplitude modulation scheme to allow high frequency detection of weak optic signals with a high signal-to-noise ratio. A DSP development system was assembled to permit programming of the DSP integrated circuit, and programming of the DSP system was begun.

- A facility for the automated fabrication of sensor probes (the Fabry-Perot assembly) was constructed and tested. The facility uses a computer-controlled three-axis micropositioning system with a spatial resolution of a few nanometers to position the sensor elements. The position of the elements is determined through the use of a white light interferometer. Two white light interferometers were designed and assembled for this research, one for use with single-mode fibers, and the other for multimode fibers. The single-mode system achieves an accuracy of 20 nm in measurement of the position of sensor elements, while the multimode system exhibits an accuracy of 3 nm. Once positioned, the glass sensor elements are fused by heat applied through irradiation by a carbon dioxide laser. The output power and duration of the laser pulses is controlled by a computer. All three subsystems of the automated fabrication facility, including the micropositioners, the white light interferometer, and the carbon dioxide laser, all can be controlled through the same computer. A graphical user interface was written to permit the fabrication process parameters to be easily changed by an operator during sensor fabrication. With the help of the automated sensor fabrication system, multimode and single-mode fiber SCIIB sensor probes can now be made in larger quantity to satisfy the immediate needs for further comprehensive tests and evaluations of the SCIIB sensors and systems.

- Using the automated sensor fabrication system, a large number of high-quality SCIIB pressure sensors were successfully fabricated. These pressure sensors had their initial air gaps and effective gauge lengths optimized for very low cross-sensitivity to temperature. To evaluate those pressure sensors, two pressure testing systems were purchased. Model 9035 pressure calibrator purchased from Pressure Systems, Inc., allows test of the resolution and accuracy of the SCIIB pressure sensor with a very high accuracy, but over a small range of pressures (up to 200 psia). The second

system is a high pressure calibration system based on the APCS controller and generator manufactured by Advanced Pressure Products, Inc., which will allow us to test accuracy, repeatability, and hysteresis of the SCIIB sensors under high pressures at elevated temperatures. The Pressure Systems calibrator has been received, and delivery of the Advanced Pressure Products system is expected in August, 1999.

- SCIIB temperature sensors were designed for operations in downhole environments. A larger number of SCIIB temperature sensors were fabricated and tested. The tests include survivability and thermal stability, differential coefficient of thermal expansion (ΔCTE), and standard deviation. Test results indicate that the sensors satisfy all the specifications required for downhole applications.

- SCIIB sensors for detection of acoustic and seismic signals were designed, using a thin diaphragm which deforms in response to the acoustic signal. Detailed analyses were performed to determine the optimal design of the frequency response and the resolution required for detection of acoustic signals. Various techniques for the bonding of the glass elements of the sensor were, among which controlled thermal bonding technologies. Encouraging progresses have been made in bonding a thin silica diaphragm to a silica. Further research work is necessary to improve the sensor fabrication techniques to make high performance acoustic sensors.

1. Specification of technical requirements

Upon the start of this program, we worked very closely with the engineers from Baker Hughes and Chevron to specify the technical requirements for the downhole measurements. The tentative specifications for sensor performance were adopted, based on inputs from Baker Hughes. These specifications, shown in Table 1.1, will be used as guidelines for sensor design and fabrication.

Sensor	Specification	Value
Temperature	range	-40 to +200°C
	accuracy	± 1.0°C
	resolution	0.01°C
	pressure	To 20,000 psia
Pressure	ranges	0 to 5,000 psia 0 to 10,000 psia 0 to 16,000 psia 0 to 20,000 psia
	accuracy	± 0.03% F.S.
	resolution	0.01 psia
	temperature	-55 to +250°C
Flow	range	0 to 100,000 barrels/day
	accuracy	10% F.S.
	resolution	0.1% F.S.
	temperature	0 to 177°C
	pressure	0 to 16,000 psia

Table 1.1. Tentative sensor specifications

2. SCIIB sensor system design and implementation

2.1. SCIIB Sensor Principle

The basic principle of the intensity-based (SCIIB) fiber sensor is illustrated in Figure 2.1. The system involves a sensor probe, an optoelectronic signal processing unit and a silica glass fiber linking the sensor probe and the signal-processing unit. The broadband light from a temperature-controlled superluminescent light emitting diode (SLD) is launched into a two-by-two fiber

coupler and propagates along the optical fiber to the sensor head. As shown in the enlarged view of the sensor head, the lead-in (input) fiber and a reflecting fiber are thermally fused to a silica glass tube with a certain air-gap separation between the two fibers. There are two partial reflections from the two fiber endfaces that forms the air gap. The two reflections travel back along the same lead-in fiber through the same fiber coupler to receiving end where the reflected light is split into two parts, one portion with the original spectrum while the other portion with a narrower spectral width. These two portions with different spectral widths are received at two photodetectors respectively. We fabricate the sensor probe in such a way that it has an initial air gap which allows only the channel with the narrow spectral width to exhibit interference fringes. As shown in Figure 2.2, when the cavity length changes, one photodetector exhibits an interference signal output while the other is relatively unchanged because the initial air-gap length is larger than the coherence length of the original source. In the signal-processing unit, we use the interferometric channel as the signal and the broadband channel as the reference. Because the two channel signals are from the same source and experience the same transmission path, they have similar behaviors in terms of source power fluctuation and fiber loss variations. Thereafter, we achieve the extremely high resolution of air gap change measurement by monitoring the interference signal, and at the same time we can compensate the source power drifting and fiber loss variations through referencing the non-inference signal from the other channel.

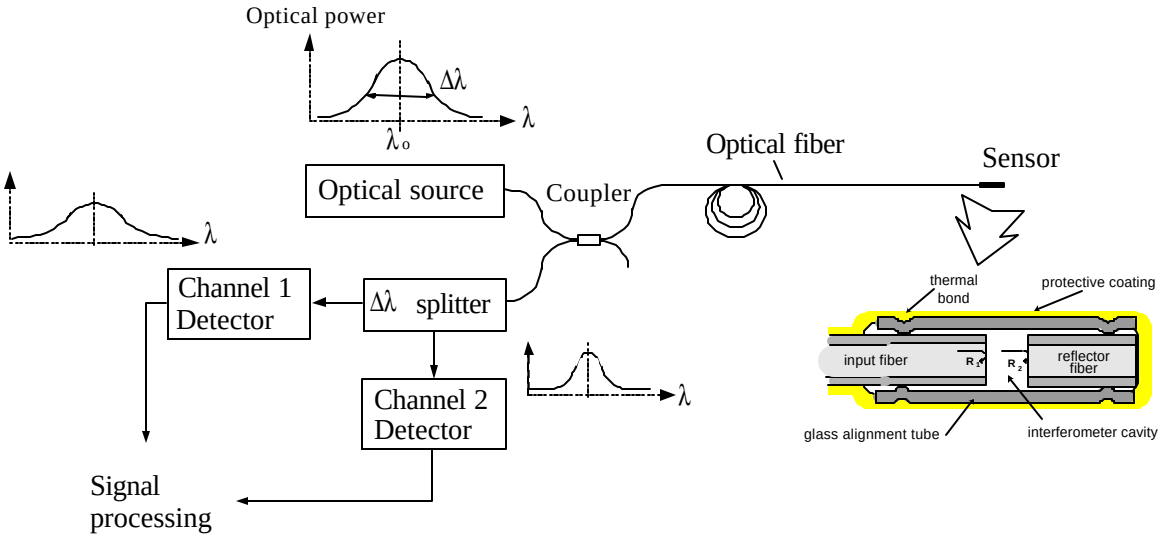

Figure 2.1. Illustration of the principle of SCIIB fiber sensor system

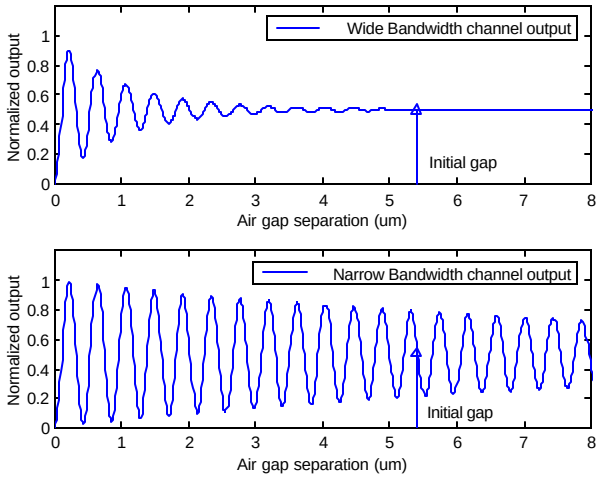

Figure 2.2. Illustration of the two channel outputs of the SCIIB sensor

In principle, continuous tracking of phase changes in the interference fringes in Channel 1 would permit measurement of air gap changes in the sensor element. Like the output of a regular interferometer, the measurement will have ultra-high sensitivity. To avoid the 2π phase ambiguity problem of normal interferometric sensors, we designed the SCIIB sensor to operate only over the linear range of a half fringe, as shown in Figure 2.3, to obtain a one-to-one quantitative relation between output intensity and the air gap separation. The SCIIB fiber optic sensor system can be used to measure different physical parameters, for instance, temperature, pressure, strain and acoustic waves. The sensor head can be specially designed to be only sensitive to the parameter of interests. In general, the measurand interacts with the sensor head and causes a change of the air gap. The SCIIB sensor system relates the air gap change to the measurand according to the physical principles governing the interaction, and directly gives the measuring results.

The above discussions indicate that the sensor possesses the advantages of both fiber interferometric and intensity-based sensors. The SCIIB sensor slices a narrow spectral band out from a broadband source, and uses this narrow band spectrum as a coherent source to obtain interference fringes. In this sense, the sensor works as an interferometer with very high resolution. The original broadband source spectrum is used as a reference for source power drifting and fluctuations in fiber attenuation. This makes self-calibration and compensation

feasible. In addition to the generic advantages offered by fiber sensor technology, such as 1) immunity to electromagnetic interference (EMI), 2) avoidance of ground loops and electric sparks, 3) remote operation, and 4) capability of multiplexing, this sensor has a number of additional advantages, including high resolution, accuracy, simple signal demodulation, absolute measurement, fast frequency response, design flexibility, and self-calibration.

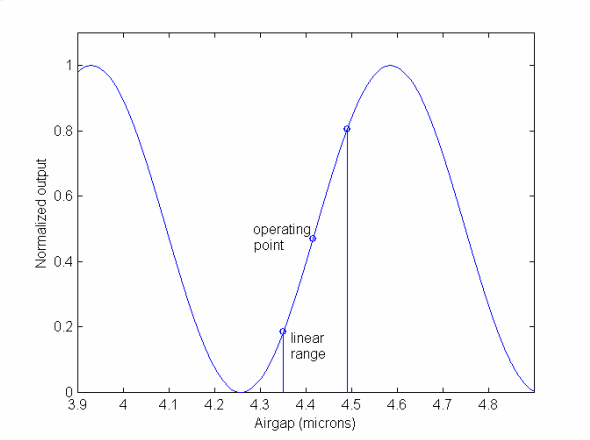

Figure 2.3. Linear operating range of SCIIB sensors

2.2. Design and fabrication of SCIIB sensor systems

Based on the above discussion, two SCIIB sensor systems were designed and fabricated. One system is multimode fiber used for short distance applications, the other is a single-mode sensor system designed for long distance applications.

The schematic of the fabricated multimode SCIIB sensor system is shown in Figure 2.4, with the actual photo of the system shown in Figure 2.5. The multimode system is designed to operate at the central wavelength of 850 nm and uses 62.5/125 standard telecom fiber. Because of the high loss of the multimode fiber at this wavelength, the system is mainly designed for short distance applications, typically less than 1km from the actual sensing region to the diagnostic center.

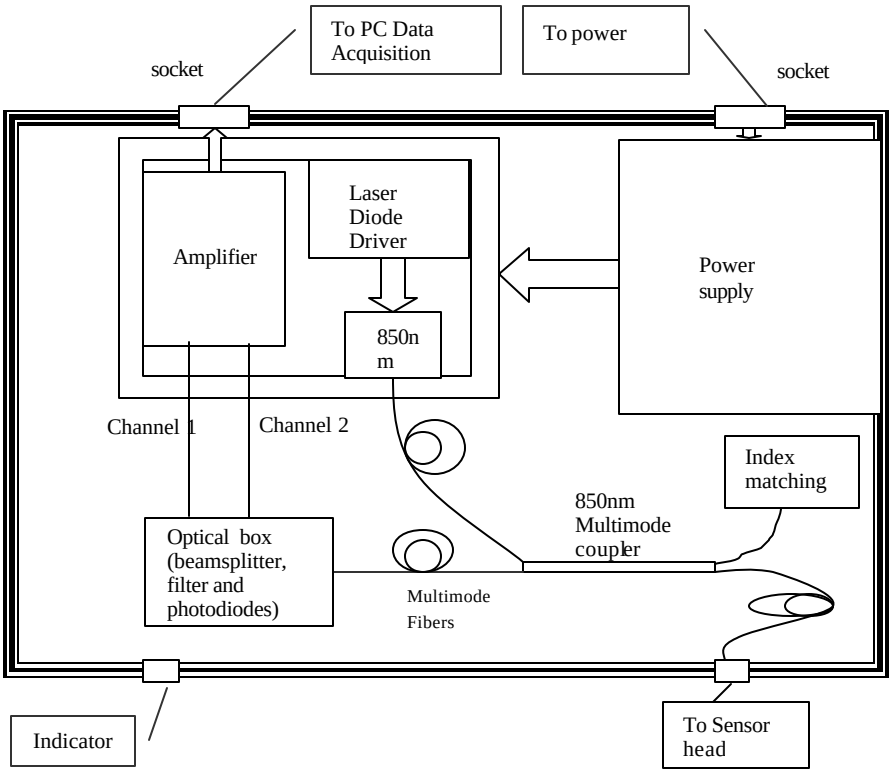

Figure 2.4 Schematic of the multimode SCIIB sensor system

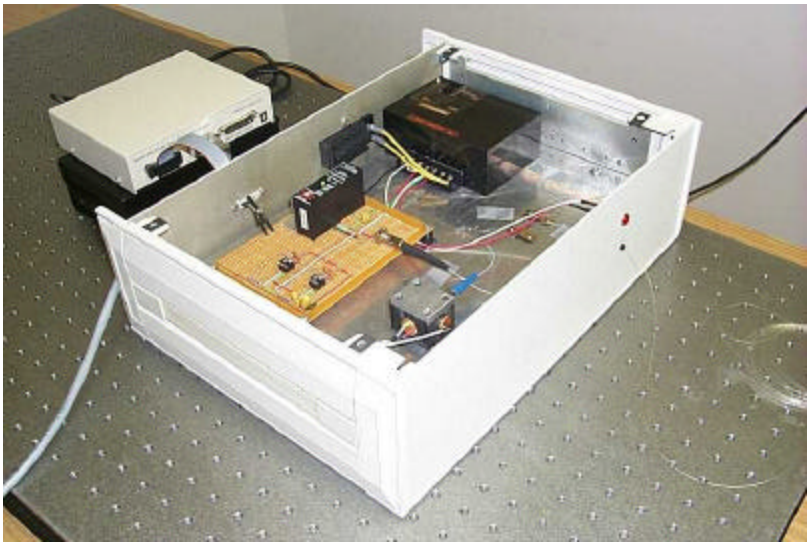

Figure 2.5. Photo of the multimode SCIIB sensor system

The schematic of the single-mode SCIIB sensor system is shown in Figure 2.6, and the actual photo of the system is shown in Figure 2.7. The single-mode SCIIB system is designed to operate at the central wavelength of 1310 nm and to use single-mode fiber to transmit optical signals between the sensor probe and the signal processing unit. Single-mode fibers have very low attenuation to the transmitted signal at 1310 nm wavelength. The system is mainly designed for long distance applications, typically longer than one kilometer from the actual sensing region to the diagnostic center.

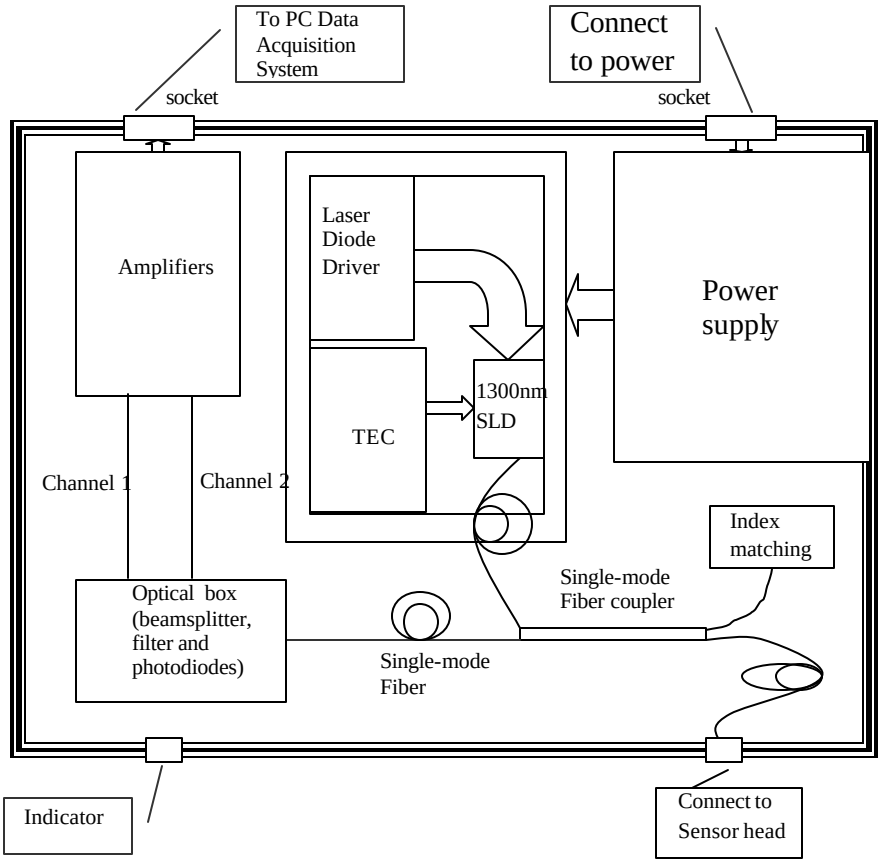

Figure 2.6. Schematic of the single-mode SCIIB sensor system

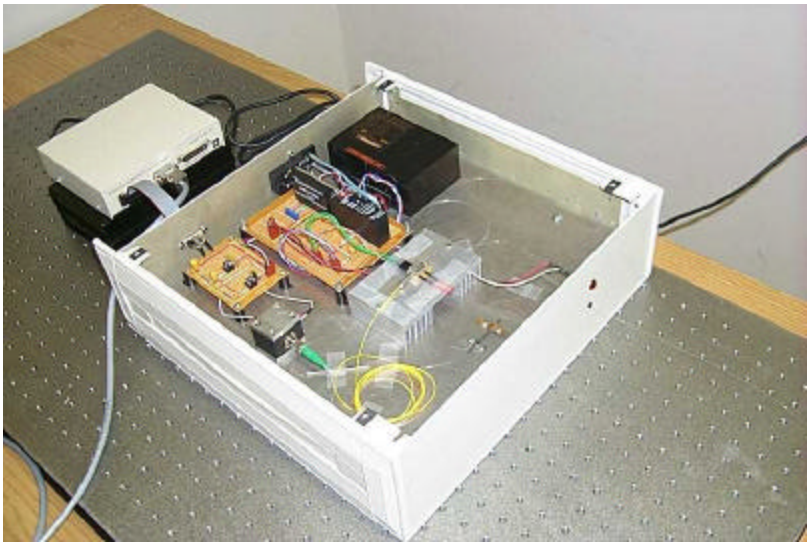

Figure 2.7. Photo of the single-mode SCIIB sensor system

2.3 SCIIB sensor system test and results

2.3.1 Self-compensation capability test

One important advantage of the SCIIB sensor is the capability of self-compensation for fiber loss variation or source output power drifting. The SCIIB sensor uses two channels with different coherent lengths for sensing and referencing respectively. The self-compensation results from the fact that the optical power received at these two channels comes from the same source and experiences the same transmission path. For instance, when fiber loss changes, it has effects on both channel outputs, and by referencing one channel output for the other, we can eliminate this fluctuation. Figure 2.8 shows experimental results of tests of the fiber loss compensation capability of the SCIIB system. The fiber used in the test was a standard telecom 62.5/125 graded index multimode fiber, and the source was an LED with the central wavelength of 851.3 nm, and a spectral width of 71.4 nm, provided by Honeywell (HEF4854-014). In the test, we introduced power loss to the system by manually bending the fiber to various diameters without changing the

sensor air gap. Two multimeters were used to record the output voltages from each channel respectively. As we expected, although the outputs of the two channels changed due to the increase of the power loss, the ratio of the two channel outputs remained the same. The sensor output ratio varied only 0.1% over the full testing range (up to 50% of the total power loss).

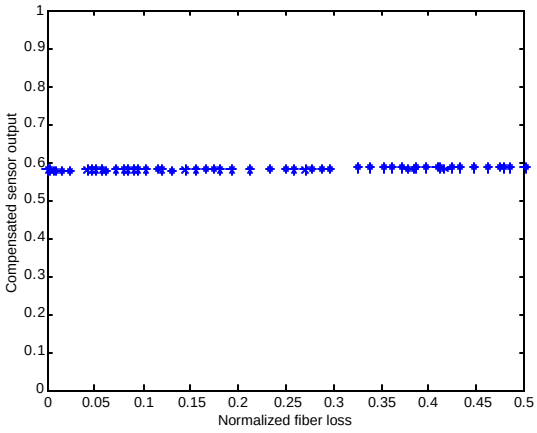

Figure 2.8. SCIIB sensor compensated output for fiber bending loss

2.3.2. Fiber bending introduced spectrum change test

The self-calibration capability of the SCIIB sensor is realized by referencing a sliced narrow spectral band interference signal to the original broadband signal. However, when single-mode optical fiber is used, the spectrum of the light waves transmitted in the fiber will change when the fiber is bent. To investigate the measurement error induced by this spectrum change, we conducted an experiment to study single-mode fiber bending.

The schematic of the experiment set-up is shown in Figure 2.9. We use an SLD as the source. The SLD was made by Anritsu Corp. (AS3B281FX) with the central wavelength of 1310 nm, the spectral width of 40 nm, and the output power of 1.21mW. The output light from the source was transmitted through a section of testing fiber, and its spectrum was studied using an optical spectrum analyzer (OSA). By manually bending the fiber to certain radii, we can study the bending introduced spectrum changes.

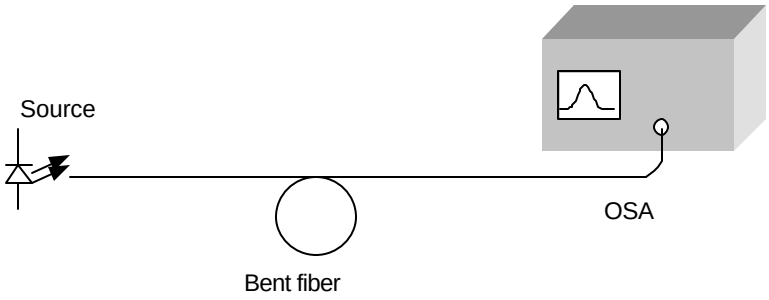

Figure 2.9. Experimental setup for fiber bending introduced spectrum change test

In the first experiment, a section of regular telecom single-mode fiber was used to run the test. The fiber was bent to successively smaller radii of 12 mm, 5 mm, 4 mm, and 3 mm respectively. The recorded spectra at these bending radii was plotted in Figure 2.10. The results indicate that the spectrum transmitted in regular telecom single-mode fiber can easily be distorted by bending the fiber. Within the spectral range of interest (1300 nm-1320 nm), the spectrum fluctuation can reach a few dB when the fiber is under severe bending, which can easily introduce measurement errors to the SCIIB system.

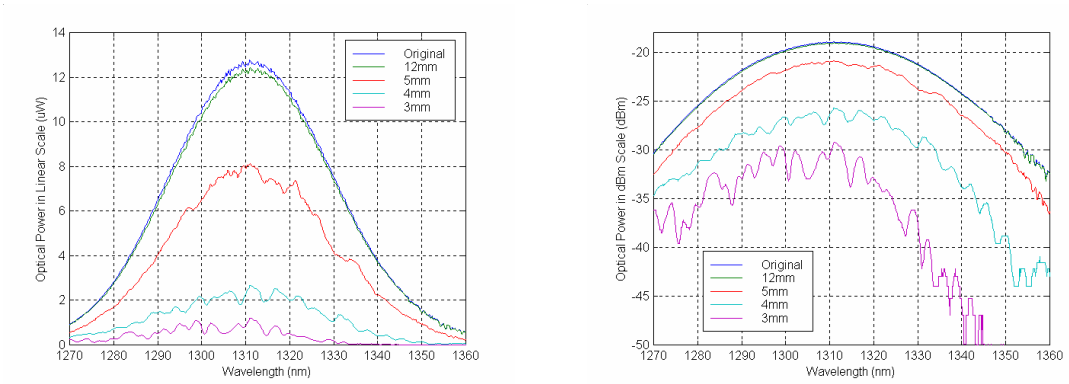

Figure 2.10. Regular telecom single-mode fiber bending induced spectrum change test results

To avoid the bending induced measurement errors, specially-designed fibers are needed in the SCIIB system. The fluctuation of the spectrum in telecom fibers is mainly due to the large mode field diameter of the waveguide. To eliminate the spectrum fluctuations, we can use bending insensitive fiber, which has a much smaller field diameter. In the second experiment, we used a section of bending insensitive single-mode fiber to repeat the above test. The fiber was purchased

from Spectran Communication Fiber Technologies, Inc., and was designed for operation at the wavelength of 1300 nm. The test results are shown in Figure 2.11. As we see, the fluctuations of the spectrum in the bending insensitive fiber are much smaller compared with that of the regular telecom fiber. Even under severe bending, the transmitted spectrum doesn't exhibit spectral fluctuations. Therefore, the experiment results suggest that the bending induced measurement errors can be minimized by applying bending insensitive fiber to the SCIIB system.

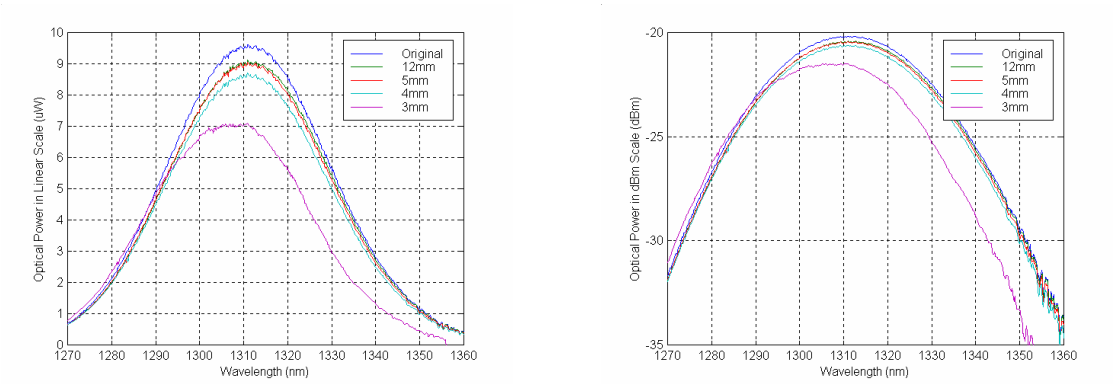

Figure 2.11. Bending insensitive single-mode fiber bending induced spectrum change test results

3. Automated SCIIB sensor fabrication system

The SCIIB fiber optic sensor system combines the advantages of both intensity-based sensors and interferometric based sensors. The full realization of those advantages requires that the SCIIB sensor must possess some unique features. These features include:

1) The initial air gap of the SCIIB sensor needs to be accurately adjusted to a certain optimal value so that the signal channel can output interference fringes with good fringe visibility while the reference channel output excludes any interference effects.
2) The initial sensor operating point needs to be precisely adjusted to the starting point of the linear portion of the interference fringe. This allows the operating range of the sensor to cover the full linear portion of the interference fringe.
3) To achieve the best thermal stability, the capillary tube and the fibers must be permanently bonded together with a high mechanical strength. Also the bonding should not have adverse effects on the optical properties of the fiber waveguide.

4) The sensor effective gauge length (the distance between the two bonding points) needs to be controlled within a tight tolerance so that the fabricated sensors have predictable and repeatable performances.
5) The fabrication of the sensor should be automatic or semiautomatic so that the sensor can be made in a large quantity with good repeatability and at a low cost.

As is well known, optical fibers are made by doping very small amount of germania to pure silica glass. Fused silica capillary tubes are also available. Silica glass is an amorphous material. When heated to a certain temperature (about 1500°C), it becomes soft and fluid. This suggests us that we can use thermal fusion techniques to bond the fiber and the capillary tube together. By locally heating the fiber and tube assembly to a temperature above the point at which the glass is softened, the tube and the fiber can flow into each other and locally join to form a solid bond.

A major achievement during this research period of the program is that we successfully developed an automated SCIIB sensor fabrication system which allows automatic fabrication of larger quantity of sensors using controlled thermal bonding techniques. In this section of the report, we present the detailed design and implementation of the automatic SCIIB sensor fabrication system.

3.1. System configuration

As shown in Figure 3.1, the automated SCIIB sensor fabrication system includes three sub-systems. They are the carbon dioxide (CO_2) laser heating sub-system, the white light fiber optic interferometric air gap monitoring sub-system, and the micro-motion positioning sub-system. A high-energy CO_2 laser is used as the heating source. It generates high-energy optical pulses at the wavelength of 10.6 μm. When the silica glass material is exposed to the CO_2 laser output, it absorbs the optical energy and converts it to thermal energy, which allows the silica glass materials be heated locally up to very high temperatures. The white light fiber optic interferometric system is used in the system to allow accurate on-line monitoring of the SCIIB sensor air gap. Several ultra-precise micro-positioning stages are also used in the system to allow precisely moving the two fibers in three dimensions. A computer is used to control and coordinate these three sub-systems so that the CO_2 laser output power, the motion of the stages and the sensor air gaps can be automatically and precisely controlled during the sensor fabrication process. Figure 3.2 shows the picture of the automated SCIIB sensor fabrication system.

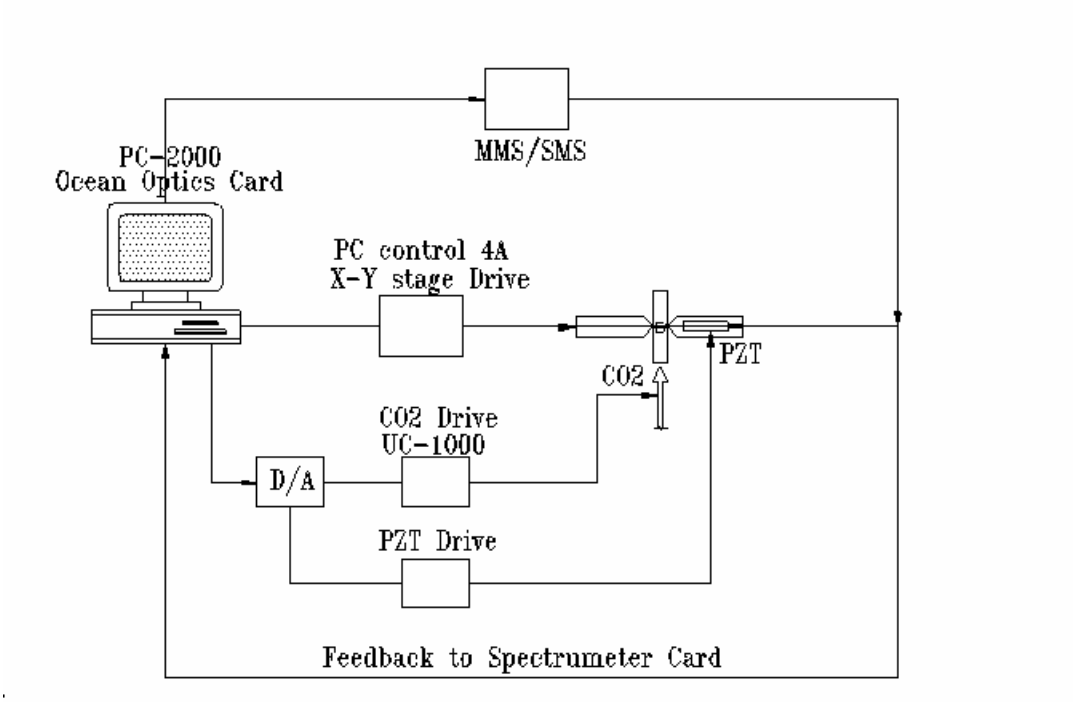

Figure 3.1. Schematic of the automated SCIIB sensor fabrication system

Figure 3.2. Picture of the automated SCIIB sensor fabrication system

3.2. CO_2 laser sub-system

The CO_2 laser used in the system is a *SYNRAD, Inc* Model 48-2. The wavelength emitted by the laser is 10.6 μm, and the maximum output optical power under continuous mode operation is 25 W. The original beam diameter of the laser output is 3.5 mm. After using a germanium lens with a focal length of 2.5 inches, a spot size of about 100 μm in diameter can be achieved at the focal point, which results in a divergence angle of about 4 milliradians. The laser can also be used to generate short optical pulses which are externally modulated through a controller, with a minimum pulse duration of about 200 μs.

The control of the CO_2 laser output involves two parts: the power level control and the lasing duration control. The power level control can be accessed by externally applying a 0-10 V voltage signal (corresponding to 0-25 W output power) and the pulse duration can be controlled by inputting a standard TTL gating signal to enable or disable the laser output. Because it is necessary to precisely control the heating time and the temperature during the sensor fabrication, we designed and implemented a special circuit to allow computer programmable control of the CO_2 laser. The block diagram of the CO_2 laser control subsystem is given in Figure 3.3. By properly programming the DIO-24 interface card (National Instruments), the power control signal is sent out to the D/A circuit, which converts the digital signal to an analog output from 0 to 10 volts at a resolution of 16 bits. The laser enabling or disabling signal is also converted to a TTL gating signal through the same circuit.

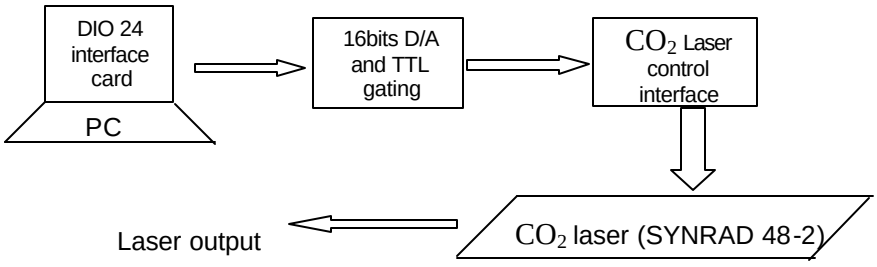

Figure 3.3 Block diagram of the CO_2 laser control subsystem

3.3 White Light optic fiber interferometer sub-system

This sub-system is the main part of the automatic sensor fabrication system. It allows on-line monitoring of the length of the SCIIB sensor air gap with a very high accuracy. The measurement of air gap length is achieved by demodulating the interference spectrum of the sensor output as described in the section below. The spectrum is obtained through a computer-interfaced spectrometer. Because we need to fabricate multi-mode and single-mode SCIIB sensors, two white light interferometric air gap monitoring systems were constructed. The two systems share the same spectrometer but use different sources and fibers.

3.3.1 Principle of the white light interferometric air gap monitoring

The basic principle of the white light interferometric air gap monitoring can be illustrated using Figure 3.4. When the sensor is fabricated, two fibers with cleaved endfaces are inserting into a capillary tube. The partially reflected optical waves at these two endfaces will generate an interference signal which is transmitted back to the spectrometer through a 2x2 fiber coupler.

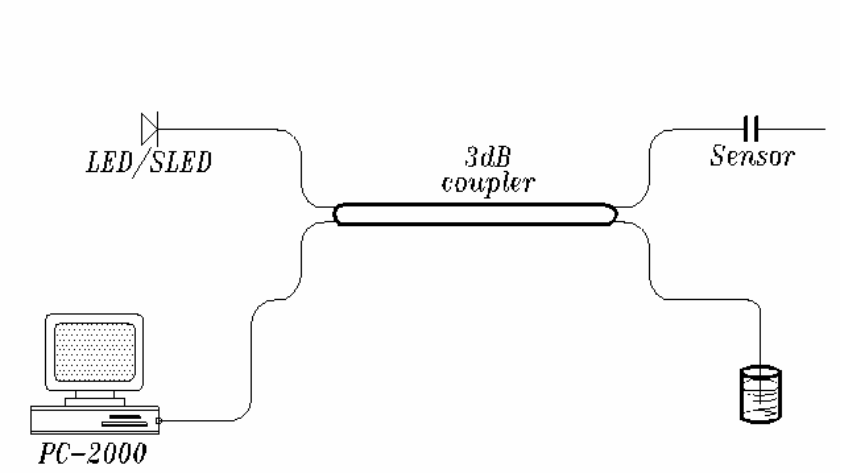

Figure 3.4 The basic principle of the white light interferometric air gap monitoring system

If we assume that the white light source (LED or SLD) has a Gaussian spectral power distribution given by

$$I_s(l) = I_0 \exp\left[\frac{-(l - l_0)^2}{(\Delta l)^2}\right] \quad , \tag{3-1}$$

where l_0 is the central wavelength, I_0 is the peak value, and Δl is the source spectral width. The output interference signal is then given by:

$$I = 2I_s(l)\left[1 + g(L)\cos\left(\frac{4pL}{l} + j_0\right)\right], \tag{3-2}$$

where the factor g takes into account the decreased visibility due to the numerical aperture of the fiber as well as other attenuating effects, and where j_0 is the arbitrary initial phase difference between the two interference signals.

If we normalize the interference spectrum given by Equation (3-2) with respect to the source spectrum, we have the normalized interference output expressed as

$$I_n = 2\left[1 + g(L)\cos\left(\frac{4pL}{l} + j_0\right)\right]. \tag{3-3}$$

It is shown in Equation (3-3) that the spectrum output by the sensor is modulated by a sinusoidal function due to the interference. Because the interference spectrum is a function of the sensor air gap length *L*, the successful demodulation of this spectral signal can render an accurate and absolute measurement of the sensor air gap length.

A simple case can be considered in which two different spectral components of the source (λ_1 and λ_2) are utilized. These two wavelength components arrive at the spectrometer with different phases, which can be expressed as

$$j_{1,2} = \frac{4pL}{l_{1,2}} + j_0 \ . \tag{3-4}$$

Thus the phase difference between these two spectral components is given by

$$\Delta j = j_1 - j_2 = \frac{4pL(l_2 - l_1)}{l_1 \cdot l_2} \ . \tag{3-5}$$

Rewriting Equation (3-5), we have

$$L = \frac{\Delta j \cdot l_1 \cdot l_2}{4p(l_2 - l_1)} \ . \tag{3-6}$$

If the phase difference of these two spectral components are known, the absolute value of the sensor air gap length *L* can be calculated by Equation (3-6).

Although it is not easy to measure the phase difference of two spectral components, there exist a few special points with fixed phase relation. For example, the phase difference between two adjacent peaks (or valleys) is 2π. Therefore, by detecting the spectral locations of the peaks or valleys in the interference spectrum, we can obtain the cavity length L by applying Equation (3-6).

3.3.2 Implementation of multimode and single-mode white light subsystems

Two white light subsystems were designed and constructed to support automatic sensor fabrication. One is designed for fabricating multimode SCIIB sensors, and the other for single-mode sensors. The two subsystems share the same spectrometer but have different sources and fibers.

The spectrometer used in the white light subsystem is a fiber optic PC plug-in spectrometer (PC2000 manufactured by Ocean Optics, Inc.). The PC-2000 spectrometer card uses a 600-line holographic grating to diffract the input light to a CCD array, and interfaces with the computer using a 12 bit A/D through the ISA bus. The blaze wavelength is 850 nm, and the best efficiency is from 750 nm to 950 nm, which covers the whole light source spectrum of interest. The resolution of this spectrometer is approximately 0.3 nm, and the highest data acquisition speed is 1000 kHz.

3.3.2.1 Multimode white light air gap monitoring system

The configuration of the multimode white light air gap monitoring system is shown in Figure 3.5. It uses an LED with central wavelength of 850 nm and spectral width of 74 nm as the source. The fiber used is a standard multimode graded index 62.5/125 telecom fiber. The picture of the system is shown in Figure 3.6.

3.3.2.2 Single-mode white light air gap monitoring system

The configuration of the multimode white light air gap monitoring system is shown in Figure 3.6. It uses a SLD with central wavelength of 1310 nm and the spectral width of 40 nm as the source. The fiber used inside the system is a standard 9/125 single-mode telecom fiber. The picture of the system is shown in Figure 3.7.

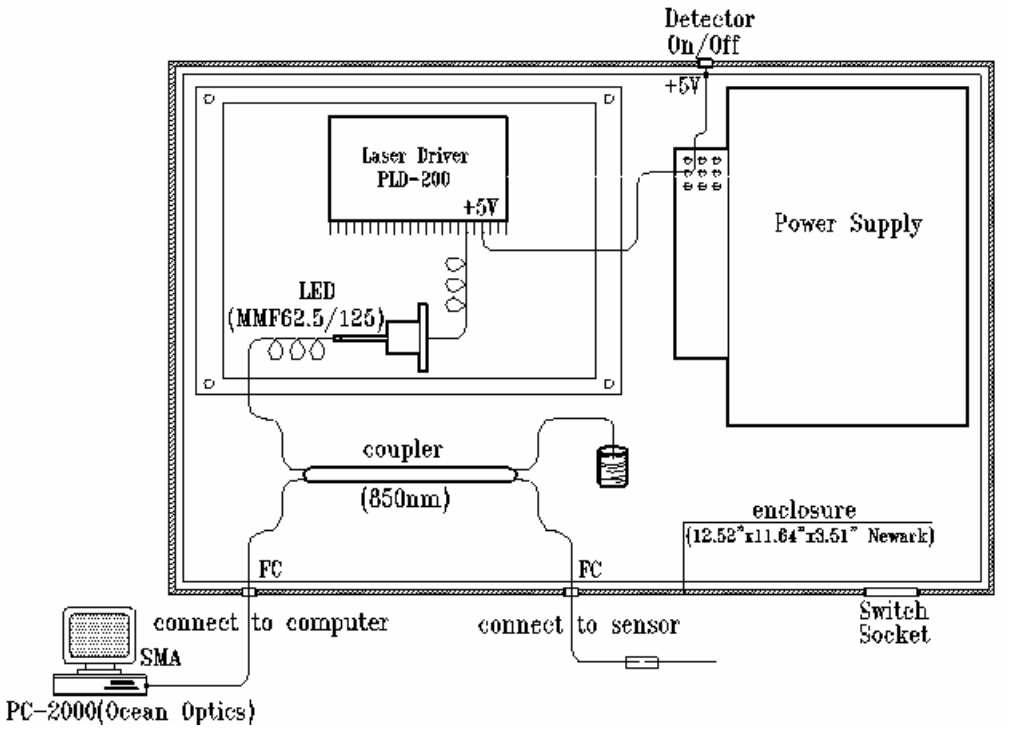

Figure 3.5. Configuration of the multimode white light air gap monitoring system

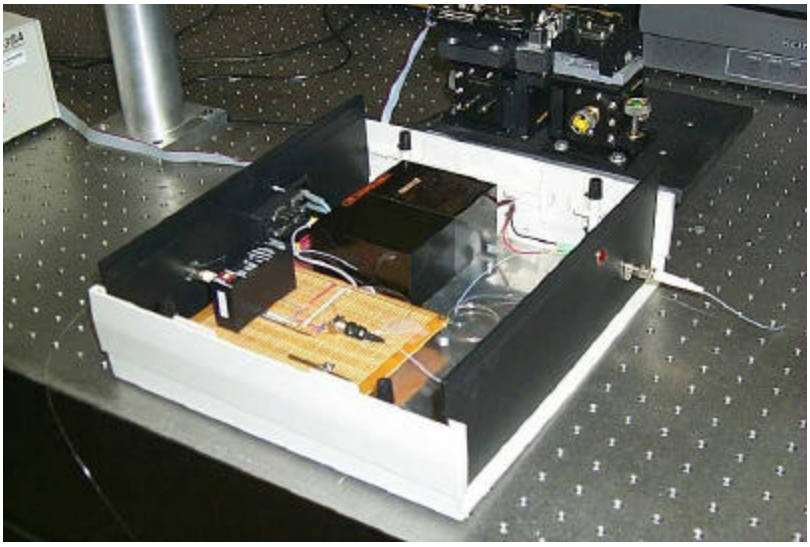

Figure 3.6. Picture of the multimode white light air gap monitoring system

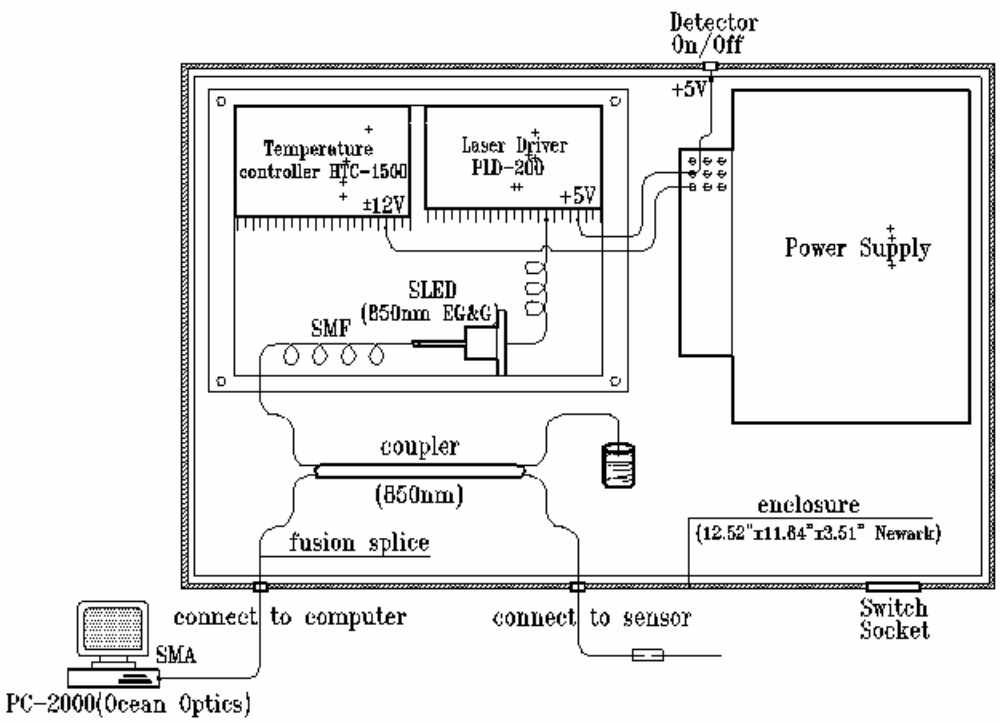

Figure 3.7. Configuration of the single-mode white light air gap monitoring system

Figure 3.8. Picture of the single-mode white light air gap monitoring system

3.3.3 Software design of white light sub-system

Advanced computer programs were developed to demodulate the interference spectral signals output from the white light subsystem so that the air gap length of the sensor can be monitored accurately while the sensor is fabricated. The computer program is based on the previous discussed phase detection method in which peaks and valleys in the interference spectrum are detected. The software is implemented in a combination of Visual Basic and C languages so that both graphic interfaces and high computational speed are achieved and optimized. The block diagram of the white light subsystem is shown in Figure 3.9. The interfaces of the designed software is shown in Figure 3.10, where (a) is the multimode case, and (b) is the single-mode case.

The major functions of this software include:

- ***Initialization***

  The program begins with the system parameter initialization, including initialization of the spectrometer, initialization of the system configuration, and initialization of the system constants necessary for the air gap calculation. The program automatically saves all the parameters of the last experiment. However, each individual parameter can also be changed manually during the operation.

- ***Pre-processing***

  The main purpose of this part is to improve the signal-to-noise ratio (SNR) of the system and improve the air gap length measuring accuracy.

  1) The dark spectrum is saved to allow only pure spectral data to be processed after the subtraction algorithm.
  2) The original spectrum of the light source is saved as the reference so that the interference spectrum can be normalized to eliminate the distortions induced by the source spectrum.
  3) A boxcar algorithm is developed to filter and smooth the raw data so that the noise of the spectrometer is minimized.
  4) The interference spectrum is automatically truncated according to its signal level. This ensures that only the high SNR region of the spectrum is included in calculations of the air gap length.

- ***Demodulation***

  This part includes the most important functions of the software.

1) The saved dark spectrum is subtracted from the input spectrum, and the saved reference spectrum is used to normalize the interference spectrum so that the source spectrum effects are eliminated.
2) Coarse locations of the peaks and valleys are found by a smart comparison algorithm. These coarse locations are used as reference marks in the demodulation.
3) An FFT algorithm is used to automatically estimate the window size of the interference spectrum. This allows an optimal number of data points to be used in the signal demodulation.
4) A mass-centroid algorithm is applied to find the interference peaks (or valleys) and the corresponding wavelengths.
5) The final air gap length is calculated according to Equation (3-6).

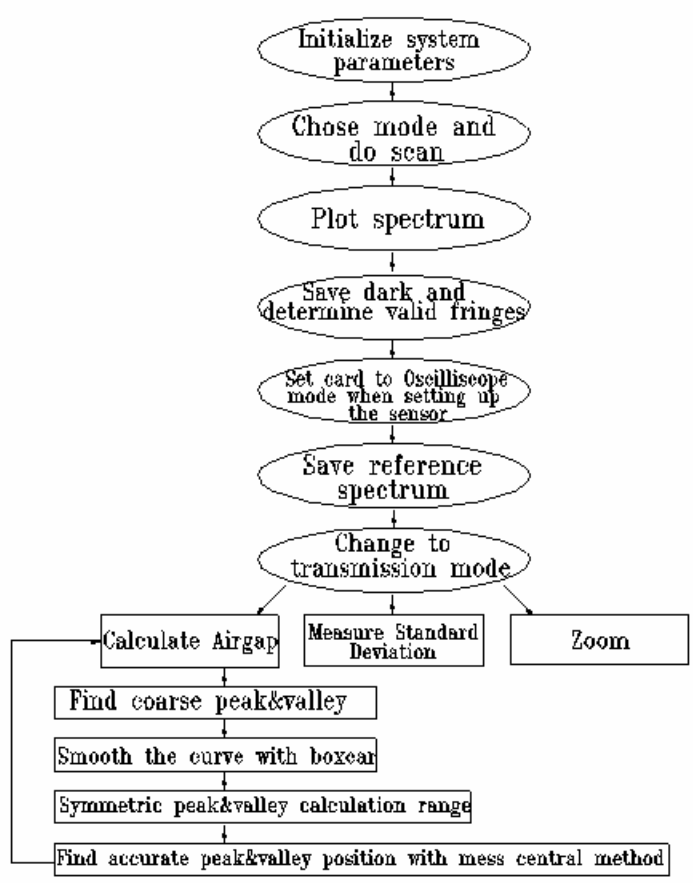

Figure 3.9. Block diagram of software

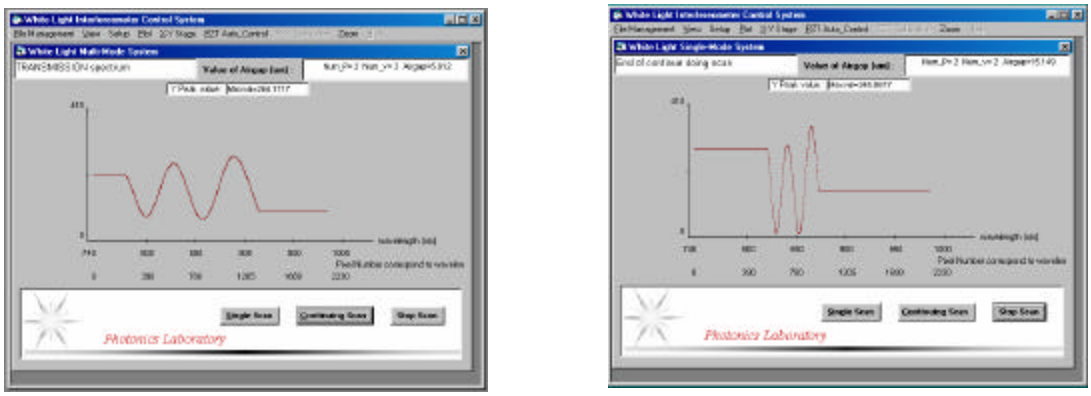

(a) Multimode (b) Single-mode

Figure 3.10. White light air gap monitoring software under operation

3.4 Micro-motion fiber positioning subsystem

During the sensor fabrication, the fibers and capillary tube must be kept precisely aligned. The sensor air gap needs to be accurately adjusted to the preset value, and the bonding distance, which determines the sensor effective gauge length, also needs to be precisely controlled. Therefore it is necessary to design a fiber positioning system for the sensor fabrication to accurately position the fibers and tubes.

The computer controlled micro-motion fiber and tube positioning system is illustrated in Figure 3.11. The two fibers are positioned on two V-grooves using magnets, and the V-grooves are fixed to a 3-dimentional translation stage, respectively. Between the two translation stages, a supporting block with another V-groove on top is used to position the capillary tube. All the V-grooves are specially designed and manufactured to hold the fibers or the capillary tube tightly. After installation, the three V-grooves are precisely aligned to fall in a straight line so that there is no offset angle during sensor fabrication. Fibers can be inserted into the central capillary tube by moving the two translation stages in three dimensions. To allow precise adjustment of the sensor air gap length, another small PZT-actuated stage is used to move the target fiber with ultra-high resolution along z-direction. The movement of the stage is controlled by the central computer through a PZT driver and a 16 bit D/A circuit. In order to control the sensor gauge length, a big translation stage is used to move the whole setup in two directions with respect to the CO_2 laser beam. After the tube is bonded to the lead-in fiber, this stage can precisely position the second

bonding point with respect to the CO_2 laser beam. A video microscope system is used to help the aligning procedure and to monitor the whole sensor fabrication process. The picture of the sensor fabrication stage system is shown in Figure 3.12.

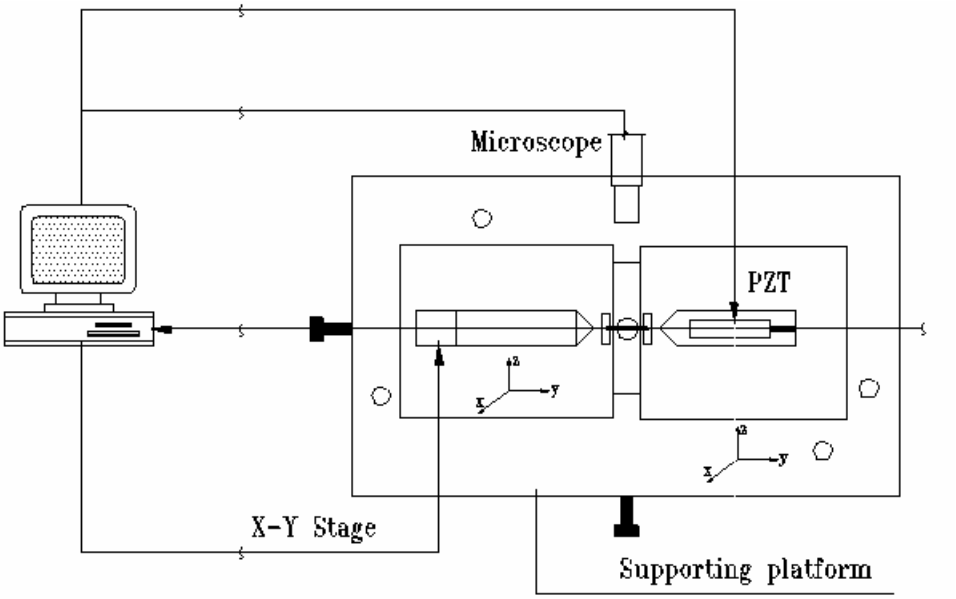

Figure 3.11. Computer controlled micro-motion fiber and tube positioning system

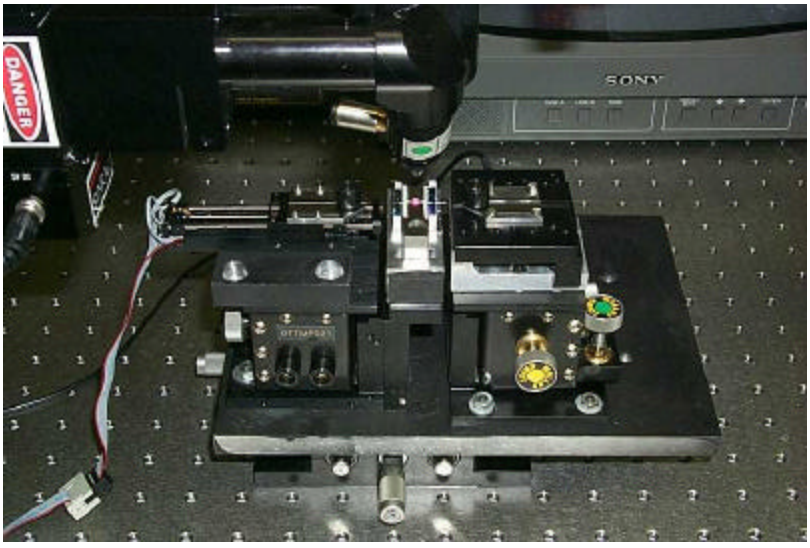

Figure 3.12. Picture of the sensor fabrication stage system

3.5 Experiments and results

Tests and experiments were conducted using the implemented automatic SCIIB sensor fabrication system. The main purpose of those experiments and tests is two-fold: 1) to verify the design and to check out the functions of each subsystem, 2) to fabricate SCIIB sensors for further evaluation.

3.5.1 White light subsystem performance test and results

The purpose of designing the white light subsystem is to realize on-line monitoring of the sensor air gap length during sensor fabrication. There are a few key performance characteristics that required tested before it could be used. These include the accuracy, dynamic range, and frequency response of the air gap measurement.

3.5.1.1 Standard deviation of the air gap measurement

The standard deviation of the white light subsystem was measured by using a fiber optic extrinsic Fabry-Perot interferometric (EFPI) sensor with a fixed air gap. Using the white light system, we measured the EFPI sensor air gap 100 times. Based on the measurement results, we can calculate the standard deviation of the white light system. Actually, this function is built in the software so that we can perform the standard deviation measurement at anytime.

The standard deviation of the multi-mode system was calculated to be $s = 0.003mm$. The standard deviation for single-mode system was found to be $s = 0.02mm$.

3.5.1.2 Frequency response test

Using the software, the sensor air gap length can be calculated in less than 0.1 second. The corresponding frequency response of the system is higher than 10 Hz. The average fabrication time of the SCIIB sensor is about 20 seconds, therefore the frequency response of the white light system is high enough for our applications.

3.5.1.3 Dynamic range of the white light system

The multimode system can measure sensor air gap lengths from 4 μm to 20 μm, and the single-mode system can measure from 8 μm to 70 μm. The standard deviation of the sensor air gap measurement is constant over the whole dynamic range. The typical initial air gap is about 6

μm for multimode and 15 μm for single-mode; therefore, the dynamic ranges of the white light system for both system are large enough.

3.5.2 CO_2 laser power calibration

The CO_2 laser is used as the heating source during the sensor fabrication. It is important to control the laser output power and exposure duration to ensure solid bonding between fibers and tube. Laser power that is too large and exposure time that is too long can result in degradation of the optical properties of the optical fiber and the too much built-in stress at the bonding region. On the other hand, laser power that is too weak or exposure time that is too short can result in incomplete bonding.

The CO_2 laser output is quite non-linear when it is controlled through the external analog port. To achieve precise control of the output power, we conducted a calibration experiment for the CO_2 laser. The laser output power was measured using a power meter. The results are plotted as shown in Figure 3.13. Based on the calibration data, the CO2 laser power can be accurately mapped to the external control voltages. Thereafter, precise control of the laser output power can be realized through curve-fitting method.

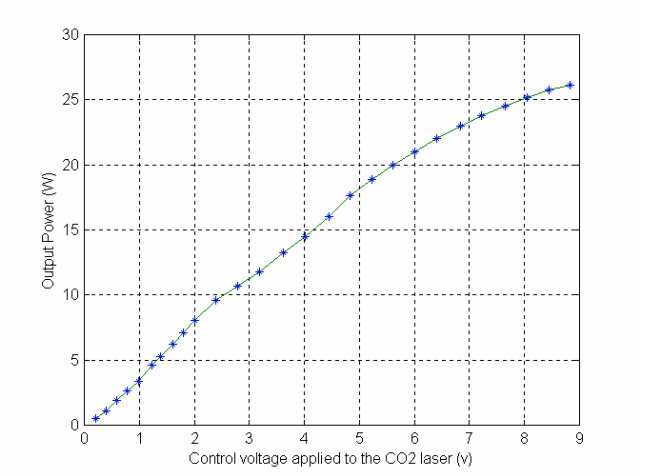

Figure 3.13. CO2 laser output power calibration results

3.5.3 PZT Stage calibration

The final fine adjustment of the sensor air gap is achieved by moving the PZT stage. The movement of the PZT stage is controlled by the computer programs through a 16 bit D/A circuit and a PZT driver. However, the relationship between the PZT displacement and the external control voltage is not linear. In order to adjust the air gap to a preset value at a ultra-high accuracy, we need to calibrate the PZT stage movement with respect to the input control voltages. The calibration was conducted by using the white light interferometer and an extrinsic Fabry-Perot interferometric (EFPI) sensor. First we implement an EFPI micro-displacement sensor with one fiber sealed to the tube, and the other fiber fixed to the PZT stage. When the PZT stage moves, it generates an interferometric displacement signal through the EFPI sensor. At the same time, this interferometric signal was measured by the white light interferometric air gap monitoring system. Relating the PZT control voltage to the white light interferometer output, the PZT stage can be precisely calibrated. Figure 3.14 shows the PZT calibration results. By using curve-fitting method, we can control the PZT stage movement with a very high accuracy by referring to the stored calibration data.

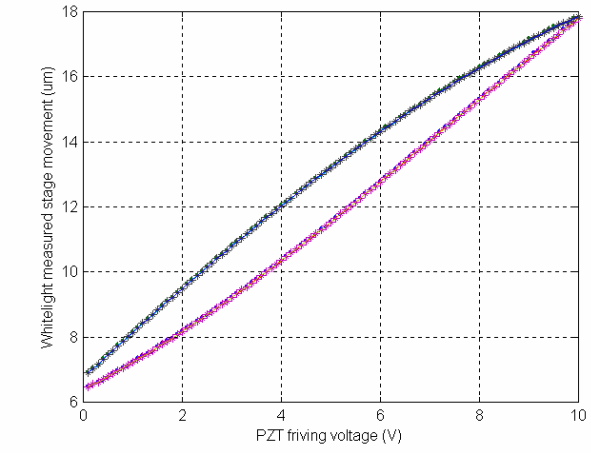

Figure 3.14. PZT stage movement calibration results

3.5.4 Sensor Fabrication

3.5.4.1 CO_2 laser power and exposure time optimization

Thermal bonding is the most important step in SCIIB sensor fabrication. When the tube and fiber assembly are exposed to CO_2 laser light, the optical energy is converted to the heat energy which results in the increase of the temperature at the exposure area. If the temperature reaches the softening point of the glass material (about 1500°C), the tube and the fiber start to flow and join together. After the cooling, a solid bond is formed at the CO_2 laser exposure area. In order to achieve the best optical and mechanical performance of the fabricated sensor, the CO_2 laser exposure time and the power level need to be set to their optimal values. There are a few points that must be considered in choosing the exposure time and the power level.

First, to avoid excess residual stress from building in the bonding area, the increase and the decrease of the temperature should not be too fast. This results in an optimal design of the temperature increasing and the decreasing slope.

Second, the glass materials should not be over-heated; otherwise the gravity will bend the fiber, which results in a large optical power loss at the bonding region. Therefore, the laser power needs to be set to an optimal level.

Third, there is an optimal time duration in which the glass materials are soft and fluid. A review of fiber optic fusion splicer design reported in the technical literature suggests that the duration at which the glass is softened should be limited to a few seconds.

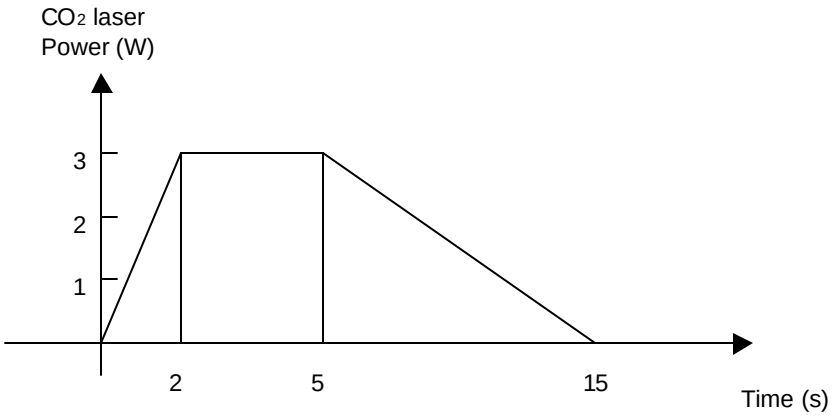

Figure 3.15. CO_2 laser power level and exposure time

Based on the above considerations, we designed our CO_2 laser power and exposure time curve as shown in Figure 3.15. This design allows 2 seconds of preheating time, 3 seconds of heating time and 10 seconds of annealing time. The total fabrication time is about 15 seconds.

3.5.4.2 SCIIB sensor fabrication and results

After many experiments and tests, we finalized all the parameters involved in SCIIB sensor fabrication. The final setup allows the tube and fiber assembly to be positioned 7.5 cm away from the CO_2 laser focal point. For multimode SCIIB sensors, the full laser power is 2.9 W, and for single-mode sensors the full laser power is 3.1 W. The sensor bonding region has a typical size of 300 μm. The sensor gauge length can be chosen from 0.8 mm to 5 mm. The initial gap can be adjusted to any value with an accuracy of 0.02 μm. The bounding points have been tested to show good strength, and the sensor fabrication has a very good repeatability.

4. SCIIB pressure sensor

Monitoring of high pressures with high accuracy in the oil reservoir is vitally important for downhole oil exploration and oil recovery applications. As proposed, one of the major tasks scheduled for the first year of the project is to investigate the application of the SCIIB fiber optic sensor configuration to pressure sensors. In this section, we report the details of SCIIB pressure sensor system design, sensor fabrication methods and the test results.

4.1 SCIIB pressure sensor design

Pressure measurement can be achieved by applying the above-discussed SCIIB fiber optic sensors. However, special considerations need to be taken in order to satisfy all the requirements for the downhole applications. The design issues include the sensor head geometry, material, sensor sensitivity, and sensor dynamic range.

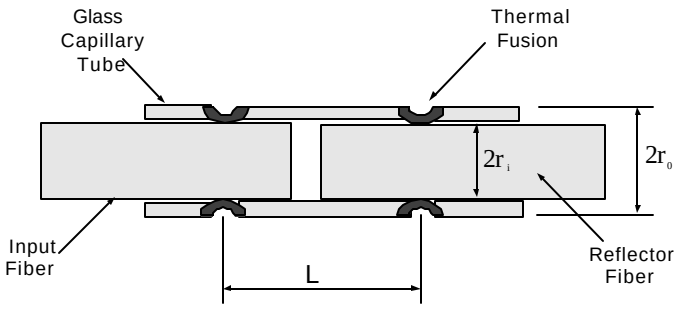

Figure 4.1. Geometry of SCIIB pressure sensor head

The geometry of an SCIIB pressure sensor is shown in Figure 4.1. The sensor head is made by inserting two fibers into a fused silica capillary tube and thermally sealing them together so that an air gap is formed between the two cleaved fiber endfaces. When a hydrostatic pressure is applied, the capillary tube will deform, and as a consequence the cavity length will change. Effects in both the longitudinal and the transverse directions should be considered.

Assume that the capillary tube has an outer radius of r_o and an inner radius of r_i. When the applied pressure changes from p_1 to p_2 the sensor air gap change (DL) can be expressed as[]

$$\Delta L = \frac{L}{E}[s_z - m(s_r - s_t)], \tag{4-1}$$

where L is the effective sensor gauge length defined as the distance between the two thermal bonding points; E is the Young's Modulus and m is the Poisson's ratio of the capillary tube. For the fused silica materials used, $E=74\ GPa$, and $m=0.17$. Three strains are concerned in the analysis: s_r is the radial strain, s_t is the lateral strain, and s_z is the longitudinal strain generated by the applied pressure. Those three strains can be calculated by the following equations:

$$s_r = \frac{(p_2 - p_1)r_o^2}{r_o^2 - r_i^2}\ (1 - \frac{r_i^2}{r_0^2})\ , \tag{4-2}$$

$$s_t = \frac{(p_2 - p_1)r_o^2}{r_o^2 - r_i^2}\ (1 + \frac{r_i^2}{r_0^2})\ , \tag{4-3}$$

$$s_z = \frac{(p_2 - p_1)r_o^2}{r_o^2 - r_i^2}\ . \tag{4-4}$$

After combining Equations (3-4) through (3-6), the cavity length change of the sensor caused by the applied pressure can be expressed as

$$\Delta L = \frac{L(p_2 - p_1)r_o^{\,2}}{E(r_o^{\,2} - r_i^{\,2})}(1-2m)\ . \qquad (4\text{-}5)$$

Equation (4-5) clearly shows that the change of the applied pressure can be measured by the change of the air gap length of the sensor. If we calibrate the sensor cavity length to a known pressure, we can measure the absolute applied pressure by measuring the change of the sensor cavity length.

As indicated above, to avoid the phase ambiguity problem, the SCIIB system requires that the sensor works over the linear range of a half interference fringe, which is approximately a quarter of a fringe. It is very important to design the sensor head so that the sensor operation is constrained to this linear range. Equation (4-5) indicates that we have the flexibility of choosing different sensor geometrical parameters to limit the measuring pressure to the linear portion of the interference fringe.

The sensor head is fabricated by inserting two fibers into a silica glass capillary tube. The tube has an inner diameter of 130 μm, which is slightly larger than the fiber cladding diameter of 125 μm. The outer diameter of the glass tube can be varied as required to achieve different dynamic ranges and resolutions according to Equation (4-5). In order to obtain good interference signals, the two fibers inside the capillary tube must be maintained in good alignment. Thereafter, the geometric parameters that can be used to modify the sensor performances are the effective sensor gauge L and the outer diameter of the capillary tube.

To further study the relationship between the sensor performances and the geometric parameters, we plot the maximum measuring pressure range versus the sensor effective gauge length and the outer diameter of the capillary tube as shown in Figure 4.2. Here we assume that the inner diameter of the tube is 130 μm and the wavelength of the source is 1300 nm. The maximum applied pressure is set to cover only the linear portion of the interference fringe which is a quarter of the source wavelength. As indicated in the plot, the change of outer diameter of the tube doesn't affect too much the sensor performance. One the other hand, the choice of the effective gauge length can allow us to design effectively the sensor to work in different dynamic ranges.

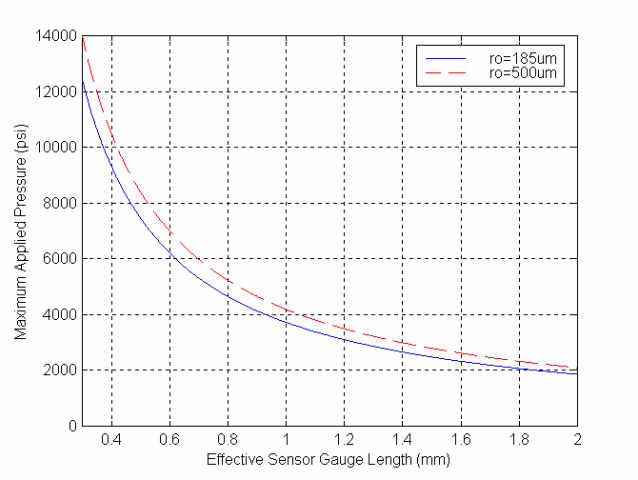

Figure 4.2. Relation between the sensor geometric parameters and the maximum pressure

4.2. Pressure sensor fabrication

Pressure sensors can be fabricated in our recently developed automated SCIIB sensor fabrication system using the controlled thermal bonding technique. After two fibers are inserted into the capillary tube and aligned to the desired initial air gap length, we thermally fuse the fibers and the tube together by locally heating them to a high temperature so that the inner tube surface and the outer surface of the fiber cladding are joined together. This thermal bonding sensor fabrication method results in two unique features of our SCIIB sensor: strong mechanical strength and high temperature stability. When the sensor is used to measure pressure, the cross-sensitivity to temperature will be minimized, due to the same thermal expansion coefficients of the tube and the fiber and the very small air gap.

There are a few important requirements that must be satisfied during the pressure sensor fabrication. First, the initial sensor air gap needs to be adjusted to the starting point of the linear portion of the interference fringe so that the operating region of the sensor covers the whole linear range of the sensor output. Second, the initial air gap need to be set to allow the signal channel to have interference fringes with good visibility while the reference channel has no interference output. Third, the effective gauge length of the sensor should be adjusted to allow the fabrication of pressure sensors with different dynamic ranges.

With the help of the white light interferometric air gap on-line monitoring system and the ultra-high resolution PZT-based micro-motion system, the air gap of the pressure sensor can be controlled with an accuracy of 4 nm, which corresponds to only 4% of the whole linear portion.

The effective gauge length adjustment can be achieved by controlling the distance between the two thermal fusion points with an accuracy of about 10 μm.

4.3. Pressure sensor testing system design

Evaluation and testing of the pressure sensors are necessary to improve the SCIIB sensor design and fabrication. However, special equipment is needed for precisely and systematically evaluating the performance of the pressure sensors.

Two pressure testing systems were designed for testing and calibrating the SCIIB pressure sensors. One system has relatively small pressure range but very high accuracy, and the other system allows us to test the sensor up to a very large pressure.

The first system is designed based on the Model 9035 pressure calibrator purchased from *Pressure Systems, Inc*. (*PSI*). The system configuration is shown in Figure 4.3. The calibration pressure range is from 0 to 250 psia, and the long-term accuracy is ±0.02% of the full range. This system would allow us to test the resolution and accuracy of the pressure sensor with a very high accuracy. A *PSI* Model 9035 pressure was ordered and received, and was interfaced to a laboratory computer for preliminary pressure testing of SCIIB sensors.

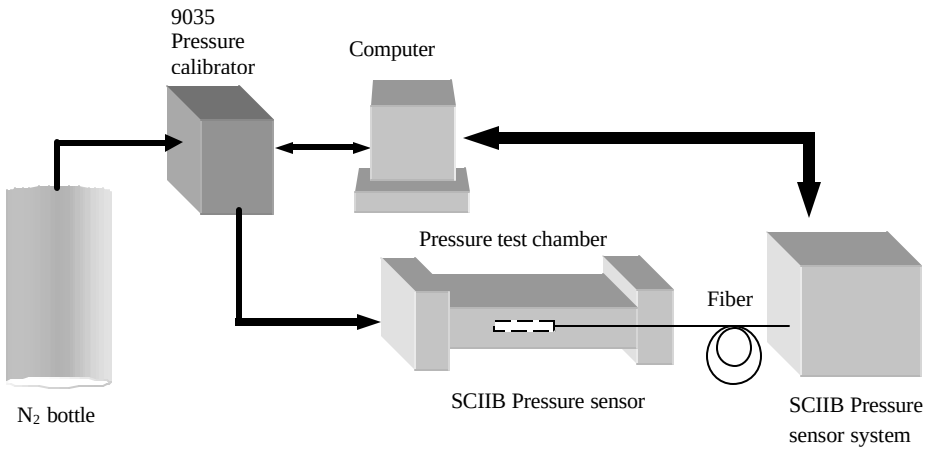

Figure 4.3. PSI 9035 based high accuracy pressure testing system configuration

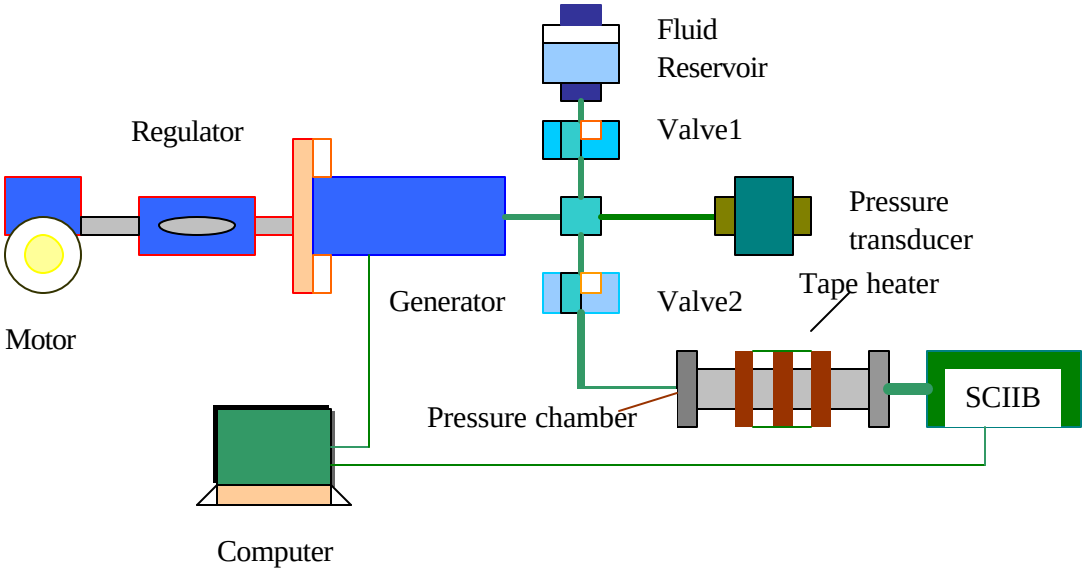

Figure 4.4 Schematic of APCS Configuration with Sensor Test System

The second system is a high pressure calibration system based on the APCS controller and generator manufactured by *Advanced Pressure Products, Inc*. The system configuration is shown in Figure 4.4. The pressure controller/generator can supply hydraulic up to 20,000 psia, and the accuracy of the pressure output is 0.02% of the full reading. The construction of this system will allow us to precisely and automatically calibrate the SCIIB pressure sensor within its whole working range. In addition, the software controlling the APCS will also test accuracy, repeatability, and hysteresis of the SCIIB sensors. The sensors can also be tested under high pressures at elevated temperatures by heating the pressure test chamber under computer control using an electrical heater.

The two pressure systems are being assembled and are under evaluation. Upon completion, we will start the complete SCIIB pressure sensor evaluation process.

5. SCIIB temperature sensor

Temperature measurement and monitoring for downhole oil recovery is another important objective in this research project. The temperature sensing can be realized through the SCIIB temperature sensor configuration. The goal of the SCIIB temperature sensor is to precisely

measure the temperature between −40ºC and +200ºC with accuracy of ±1.0ºC and resolution of a 0.01ºC under pressure up to 20,000 psia. In this section, we present the detailed design on the SCIIB temperature sensor system, including the sensor geometric design, sensor fabrication, sensor testing, calibration and characterization.

5.1 SCIIB temperature sensor design

The geometry of the SCIIB fiber optic temperature sensor can be illustrated using Figure 5.1. The structure of the temperature sensor resembles that of the pressure sensor except the difference of the geometric parameters and the material used for the alignment tube. When the ambient temperature changes, the physical length of the capillary tube and the fibers will change, which results in the change of the air gap between the two fiber endfaces. Using SCIIB system, this air gap change can be detected through the output ratio of the two channels, and thus enable precise measurement of the temperature.

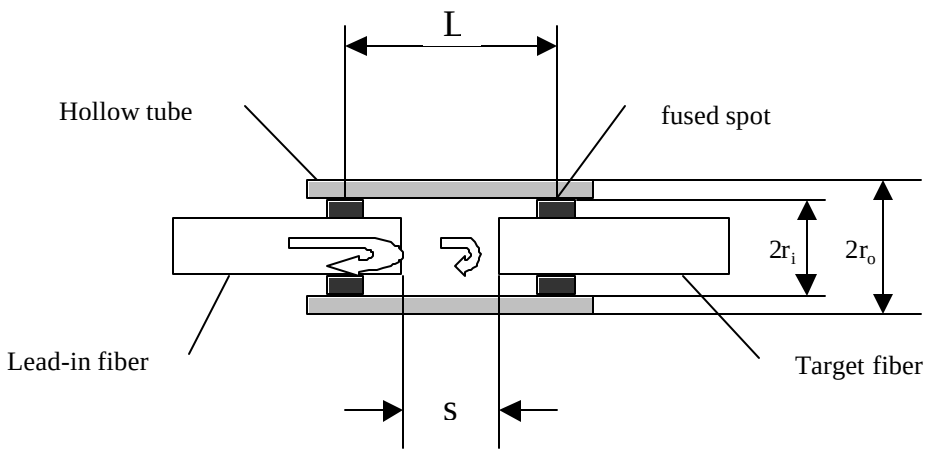

Figure 5.1. Geometry of SCIIB temperature sensor

As shown in Figure 5.1, assume that the effective sensor gauge length is *L* and the air-gap length is *s*. If the capillary tube is chosen to have a coefficient of thermal expansion (CTE) of α_h, and the CTE of the fibers is α_f, then the temperature introduced air gap length change Δs can be calculated by

$$\Delta s = [(\alpha_h - \alpha_f)L + \alpha_f s]\Delta T, \tag{5-1}$$

where ΔT is the temperature change.

Since usually L>>s, the above equation can be simplified as

$$\Delta s = \Delta \alpha L \Delta T, \tag{5-2}$$

where $D\alpha = \alpha_h - \alpha_f$ is the differential coefficient of thermal expansion (ΔCTE) of the sensor.

Equation (5-2) indicates that the air gap change Ds is proportional to the ΔCTE of the sensor and the effective gauge length. This can be used to optimize the design of our SCIIB temperature sensor. The capillary tube is chosen to be made of fused silica glass, which has a CTE of $\alpha_h = 5.5*10^{-7}/°C$. The fiber is made by doping small amount of germania into pure silica material. Typical fibers have a CTE of about $7.5*10^{-7}$/°C, which is very close to that of pure silica. Similar to the pressure sensor design, we plot the maximum temperature measurement range versus the sensor effective gauge length as shown in Figure 5.2. Here, we assume that the source wavelength is 1300 nm, the fiber is single-mode fiber, and the maximum temperature change generates a gap change corresponding to 1/8 of the source wavelength, which covers the whole linear range of the interference fringe. As we see, the maximum measuring temperature decreases with the increase of the effective gauge length. The sensor can be designed to have a maximum temperature measuring range from 100°C to 800°C when it is fabricated to have a gauge length from 1 mm to 8 mm.

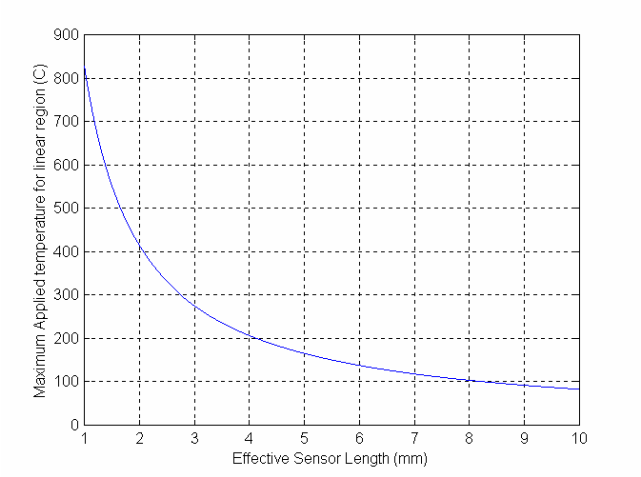

Figure 5.2. Relationship between sensor parameters and the temperature measuring range

5.2. SCIIB temperature sensor fabrication

The SCIIB temperature sensor can be fabricated on the previous mentioned automated sensor fabrication station. The fabrication process involves inserting two cleaved fibers inside a capillary tube and using the CO_2 laser to thermally fuse the fibers and the tube together. We choose fused silica material to make the capillary tube. In our experiments, we used the fused silica capillary tube available from Polymicro Technologies, Inc. The inner diameter of the tube is 130 μm, and the outer diameter is 365 μm.

The SCIIB temperature sensor fabrication requires precise control of the initial gap so that the sensor has an initial operating point at the starting point of the linear portion of the interference fringe. The sensor effective gauge length can also be controlled during the fabrication by use a translation stage to move the bonding point with respect to the CO_2 laser beam. After the sensor is fabricated, another duration of CO_2 laser exposure is applied to provide proper annealing to the bonding region so that the residual stress can be removed.

5.3. Experiments and results

5.3.1. Sensor thermal survivability and stability test

An important issue for investigation is the robustness and stability of the SCIIB temperature sensor under conditions representative of the downhole environment. To answer this question, we conducted an experiment to test the sensor survivability under high temperature. The experiment set-up includes an electrical furnace which has a maximum temperature up to 1100°C, with an Omega CN76000 thermometer to read the temperature at an accuracy of 0.1°C. The SCIIB fiber optic sensor and the thermometer were put side by side in the oven, and the temperature was increased from room temperature to 900°C in steps of 10°C. Both the SCIIB sensor output and the thermometer output were recorded for comparison. The temperature sensor under test had an effective gauge length of 1 mm, and the initial air gap of 5.93 μm. The temperature sensor was tested in the furnace several times. The test results are plotted in Figure 5.3. As we see, the sensor successfully survived the test and the output was quite repeatable. The testing results also indicates that the sensor has a very good thermal stability.

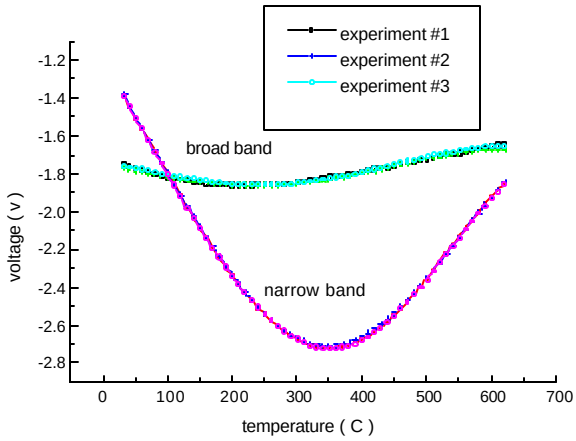

Figure 5.3. Temperature sensor survivability and stability test results

5.3.2. Test of the differential coefficient of thermal expansion (DCTE)

The ΔCTE is an important parameter in designing the dynamic range of the SCIIB temperature sensors. Theoretically, the ΔCTE of the sensor can be calculated by referring to the nominal CTEs of the tube material and that of the fibers. However, the actual CTEs of the fiber and the tube can deviate from their theoretical values due to the small chemical or physical differences among the materials used by different manufacturers. Therefore, the precise value of the ΔCTE can only be known experimentally.

In order to measure the ΔCTE of the SCIIB sensor assembly, we fabricated another sensor with an effective gauge length of 2.5 mm, and the initial air gap length of 5.75 μm. The sensor was tested using the same experimental set-up as described in the survivability test. The sensor output versus the increase of the temperature is plotted in Figure 5.4. Because the sensor has a gauge length longer than the first sensor, when temperature increases, the air gap change can cover more than half of an interference fringe. We know that the change from the peak to the valley of an interference fringe corresponds to an air gap change of a quarter of the wavelength; therefore, the ΔCTE can be calculated by finding out the corresponding increase of the temperature between these two points. We used the multimode SCIIB system during the experiments, which has a source central wavelength of 850 nm. The temperature increase from the peak point to the valley point is ΔT=420°C. Therefore, according to equation (5-2), the ΔTEC of the sensor is 2.0238×10^{-7}/°C.

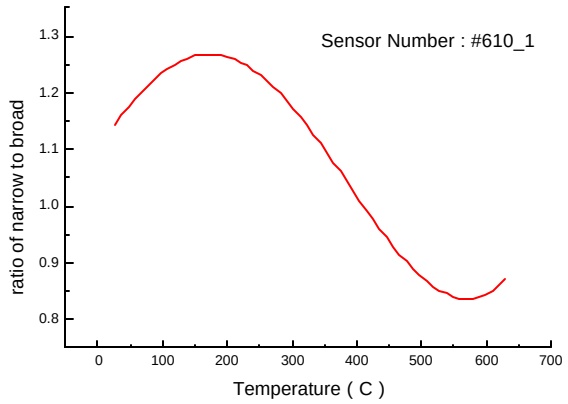

Figure 5.4. Test result used for calculating the ΔCTE of the sensor

5.3.3. Temperature sensor standard deviation test

The standard deviation of the temperature measurement has been tested. In this test, we kept the SCIIB temperature sensor in a controlled environment with a constant temperature. After the temperature of the environment was stabilized, we continuously measured the ambient temperature 100 times. The sensor used in this experiment was a multimode sensor with an effective gauge length of 2 mm and an initial air gap of 5.6 μm. The deviations of those measured data is plotted in Figure 5.5. Based on these data, we conclude that the standard deviation of temperature measurement is $\sigma = 0.0044°C$.

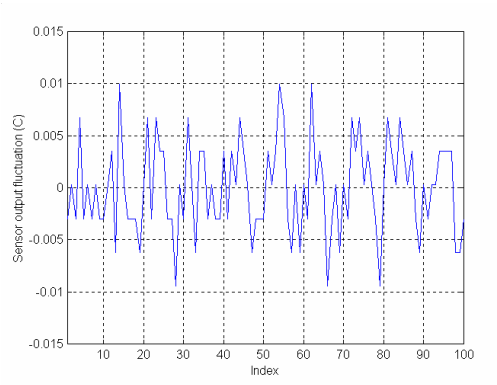

Figure 5.5. SCIIB temperature sensor standard deviation test results

6. Acoustic sensor design and implementation

Acoustic (or seismic) signals are another very useful information in downhole oil recovery. The acoustic wave can generate very small pressure when it is propagating in the oil reservoir, therefore, the detection of the acoustic wave signals can be realized by high sensitivity and high frequency response fiber optic pressure sensors. In this section, we will focus on report of the design and implementation of the acoustic sensors.

6.1 Principle of Operation

The basic principle and configuration of the fiber optic acoustic sensor can be illustrated using Figure 6.1. The system consists of a sensor probe, a light source, an optoelectronic signal processing unit, and an optical fiber linking the sensor probe and the signal-processing unit. As shown in the enlarged view of the sensor head, the input fiber and the thin silica glass diaphragm are bonded together in a cylindrical silica glass tube to form a Fabry-Perot sensing element.

Figure 6.2 illustrates the principle of operation of the diaphragm-based fiber optic acoustic sensor. The small pressure generated by an acoustic signal causes a deformation of the diaphragm and modulates the sealed air gap length. The sensor therefore gives outputs that correspond to the acoustic signals. Like regular interferometers, the measurement will have ultra-high sensitivity. On the other hand, however, the measurement would suffer from the disadvantages of sensitivity reduction and fringe direction ambiguity when the sensor reaches peaks or valleys of the fringes. One of the key successes of our sensor is that a controlled bonding technique is used to fabricate the acoustic sensor so that the sensor operates only over the linear range of a half fringe. As shown in Figure 6.2, the initial operating point is chosen to be the central point of the interference fringe, and the thickness of the diaphragm is designed in such that the imposed acoustic signal only deforms the thin diaphragm within the linear part of the sensor response curve. Therefore the sensitivity reduction and fringe direction ambiguity problems can be completely avoided.

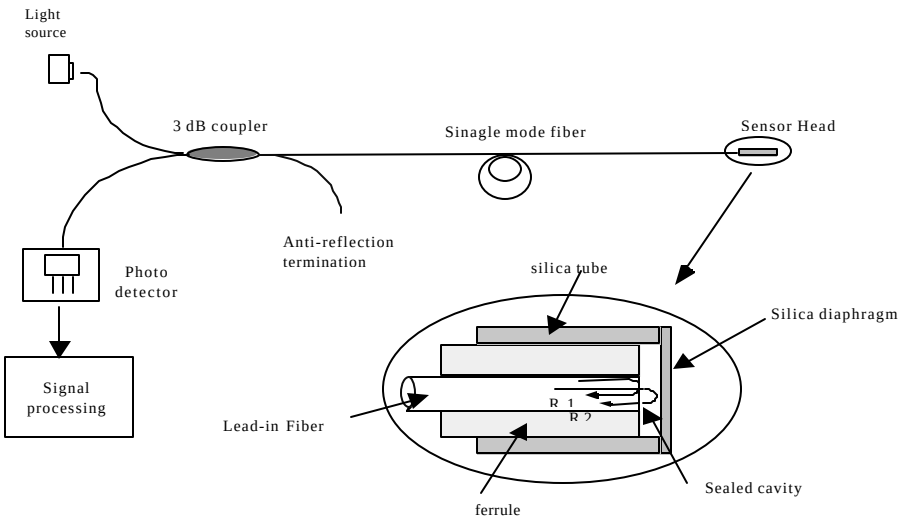

Figure 6.1 Illustration of the principle of the fiber optic acoustic sensor.

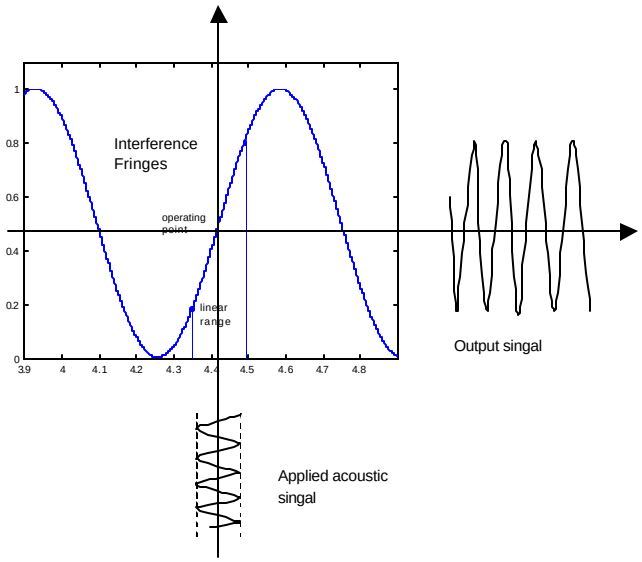

Figure 6.2 Illustration of a linear operating range of the sensor response curve.

6.2. Sensor frequency response and sensitivity design

We can use the structure shown in Figure 6.3 to model the acoustic sensor. The diaphragm vibrates at the presence of an acoustic wave when it imposes a dynamic pressure on the

diaphragm. It is very important to design the sensor head to ensure high enough frequency response and sensitivity to achieve optimum detection of the acoustic signals.

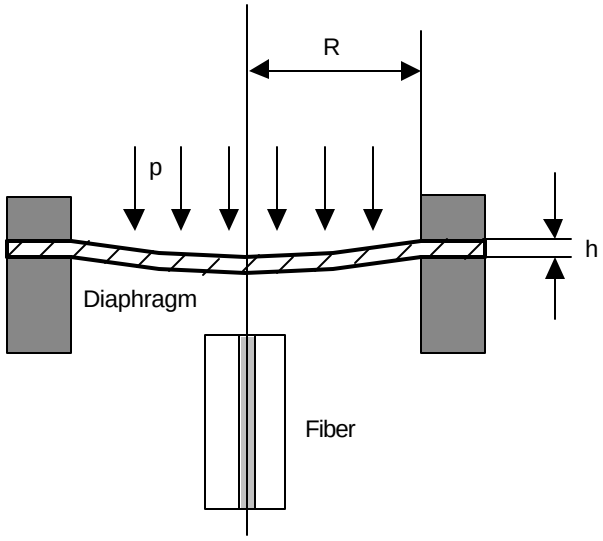

Figure 6.3 Structure model for diaphragm-based acoustic sensor

The frequency response of the sensor is limited by natural frequency (f_n) of the diaphragm. The natural frequency can be calculated by the following equation[3]:

$$f_n = \frac{a}{2pR^2} \times \sqrt{\frac{Dg}{hw}} \quad , \tag{6-1}$$

where α is a constant related to the vibrating modes of the diaphragm, and takes a value of 10.21 for the fundamental mode; R is the effective radius defined by the inner diameter of the silica sensor-housing glass tubing; h is the thickness of the diaphragm; g is the gravitational constant; w is the specific weight of the diaphragm material (for fused silica at 25 C°, 2.202×10^3 kg/m^3); and D is the flexural rigidity of the diaphragm defined by

$$D = \frac{Eh^3}{12(1-m^2)}, \tag{6-2}$$

where m is the Poisson's ratio (m = 0.17 for silica glass material at 25°C); E is the Young's modulus of the silica glass material (E = 73.73 GPa or 7.49×10^9 kg/m^2 at 25°C); The frequency response of the sensor can thus be calculated by combining Equations (6-1) and (6-2) into

$$f_n = 2.749\times10^9 \frac{h}{R^2} \text{ (Hz)}, \tag{6-3}$$

where h and R are in microns.

As indicated by Equation (6-3), the frequency response is proportional to the thickness of the

diaphragm and inversely proportional to the square of the effective diaphragm radius. If we choose the diaphragm with the effective radius of 0.5 mm, we can plot the predicted frequency response of the sensor as a function of diaphragm thickness as shown in Figure 6.4.

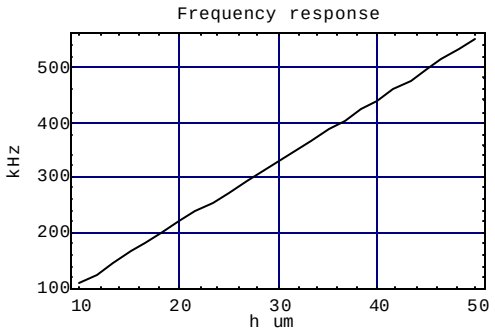

Figure 6.4 Predicted frequency response of the sensor at $R=0.5$mm

The diaphragm will be deflected when there is a differential pressure p between the inside and outside of the sealed cavity. The out-of-plane deflection of the diaphragm y as a function of the pressure difference at any radial position r is given by[3]

$$y = \frac{3(1-m^2)p}{16Eh^3} \times (R^2 - r^2)^2 . \tag{6-4}$$

In our sensor configuration, the fiber is positioned to the central part of the diaphragm so that only the center deflection y_0 is of interest, which is given by

$$y_0 = 1.71 \times 10^{-8} \frac{R^4}{h^3} p , \tag{6-5}$$

where again, y_0, R and h are all in microns, and p is in the pounds per square inch (*psia*).

From the above equations, it is seen that the sensitivity of the sensor can be designed to fit different application requirements either by choosing diaphragm materials with different m and E or by changing the geometric parameters of the sensor head with desired effective diaphragm size R and thickness h. In general, a diaphragm with a larger radius and a smaller thickness will render more sensitive detection of the acoustic signals. However, as indicated above, the operating range of the acoustic sensor head needs to be limited within the linear range, which is a fraction of an interference fringe in order to avoid the sensitivity reduction and fringe direction ambiguity problems. This imposes a limitation on the thickness of the silica diaphragm. Figure

6.5 shows the sensor response predicted by Equation (6-5).

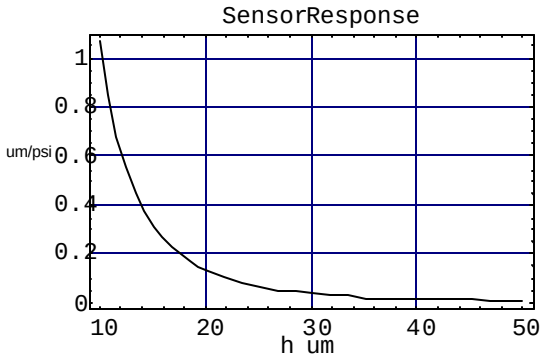

Figure 6.5. Predicted sensor response (μm/psia) versus diaphragm thickness at *R=0.5* mm.

6. 3 Acoustic sensor fabrication

As addressed above, the pressure sensor head is fabricated delicately by bonding silica fiber, ferrule, tube and diaphragm together to form an interferometer with sealed cavity. To achieve high temperature stability, solid bonding is necessary among these four components. There are several challenging requirements in the acoustic sensor fabrication. First, the fabricated sensor should have an initial air gap allowing the sensor operating point to be located in the linear part of an interference fringe. This requires precise air gap control and adjustment during the sensor fabrication. Second, the sensor operation requires a stable operating point to eliminate the sensitivity degradation and phase ambiguity problem. Therefore, the components used to make the acoustic sensor need to be made of the same or closely matched material so that the thermal stability of the sensor is ensured. Third, the sensor is intended to be used in the downhole environments; therefore the overall size of the sensor needs to be very small. To satisfy those special requirements, we investigated several sensor fabrication techniques including the epoxy-based sensor fabrication, the solder bonding method, and the controlled thermal bonding method. Although the first two methods appear to be relatively easy, the sensor performance doesn't satisfy the requirements. We therefore focused our research effort in the third method: controlled thermal bonding techniques.

6.3.1 Direct bonding method

The mechanism on which the direct thermal bonding method is based is similar to that of the SCIIB sensor bonding. When two glass materials are put close to each other and heated to a high temperature, the two pieces start to flow into each other. After cooling, the two pieces will join together to form a solid bonding. When using thermal bonding for sensor fabrication, it is very important to have precise temperature control. Temperatures that are too high could melt the material and damage the structure of the components. On the other hand, temperatures that are too low could result in false bonding.

Using methods similar to the SCIIB sensor fabrication, we use a CO_2 laser as the heating source to fabricate the acoustic sensor because of the small sensor size and the ability to focus the laser output to a small spot. Silica glass materials have very high absorption coefficient at the typical CO_2 laser wavelength (10.6 μm). The optical energy will be transferred to heat, and will raise the temperature, and eventually reaching the softening point of the glass material.

The system setup is shown in Figure 6.6. The CO_2 laser, with a maximum output power of 25 W, was purchased from Synrad Inc. The precise control of the CO_2 laser exposure duration and the output power is achieved by a computer controlled D/A circuit and the laser controller box. A computer controlled precision stage platform is also used to position the sensor head assembly with respect to the focused CO_2 laser beam.

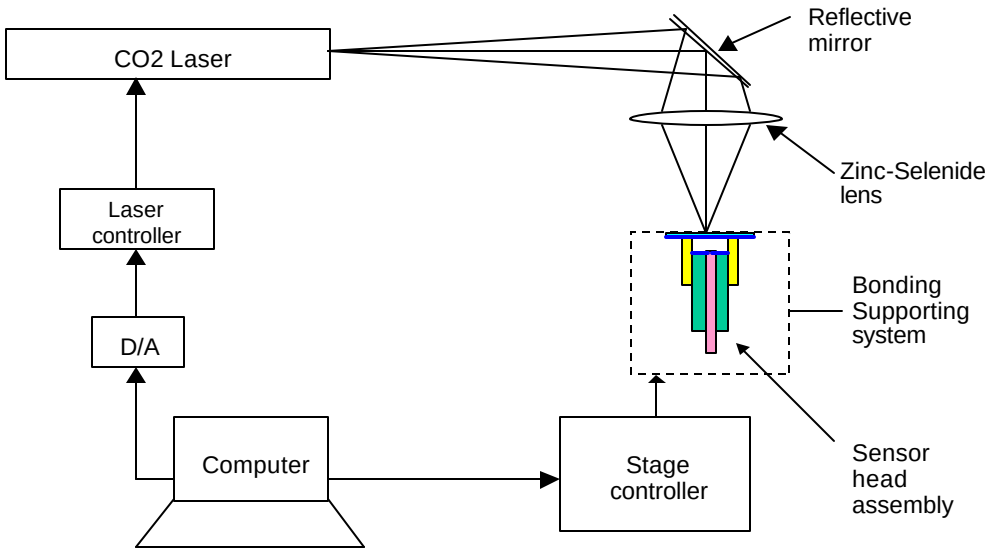

Figure 6.6. Direct thermal bonding diaphragm-based acoustic sensor fabrication system

Currently, we have successfully bonded the fiber to the ferrule with a very small attenuation (<10%) to the reflected optical power. Development is still continuing on bonding the ferule to the tube, and bonding the diaphragm to the tube.

6.3.2 Intermediate layer method

Previous experiences on epoxy-based sensor and soldering-based sensor fabrication suggests that we can use a more rigid intermediate material between two pieces of fused silica materials to achieve solid bonding.

Borosilicate glass and soda lime glass have much lower softening points (720°C and 696°C respectively) than the fused silica glass (1585°C), but higher than the operating temperature of most epoxies and solders. If we apply these intermediate materials between two pieces of fused silica materials, and heat them up to a certain temperature higher than the softening point of the intermediate layer but lower than that of the fused silica glass, the intermediate layer will become fluid, holding the two fused silica pieces together to form a rigid bond. A thin layer of the intermediate material will not significantly degrade the sensor performance.

Based on the above discussions, we designed an acoustic sensor fabrication system by applying the intermediate layer method. The system configuration is shown in Figure 6.7. In the system, a furnace is used as the heating source. The sensor assembly, with intermediate layer materials applied to the bonding region, is precisely positioned inside the furnace to allow uniform heating. A thermocouple is placed close to the sensor assembly so that the temperature can be precisely controlled and monitored during the sensor fabrication. The ferrule, fiber and the tube can be bonded together by applying borosilicate powder. The bonding between the tube and the diaphragm is then achieved by using a special thin borosilicate fiber ring. The diaphragm is held before bonding by a vacuum tool. The holder for the ferrule and tube is made of fused silica glass which has the same thermal expansion as the sensor components. After the sensor is bonded, it is necessary to anneal it for few hours to release the residual stress.

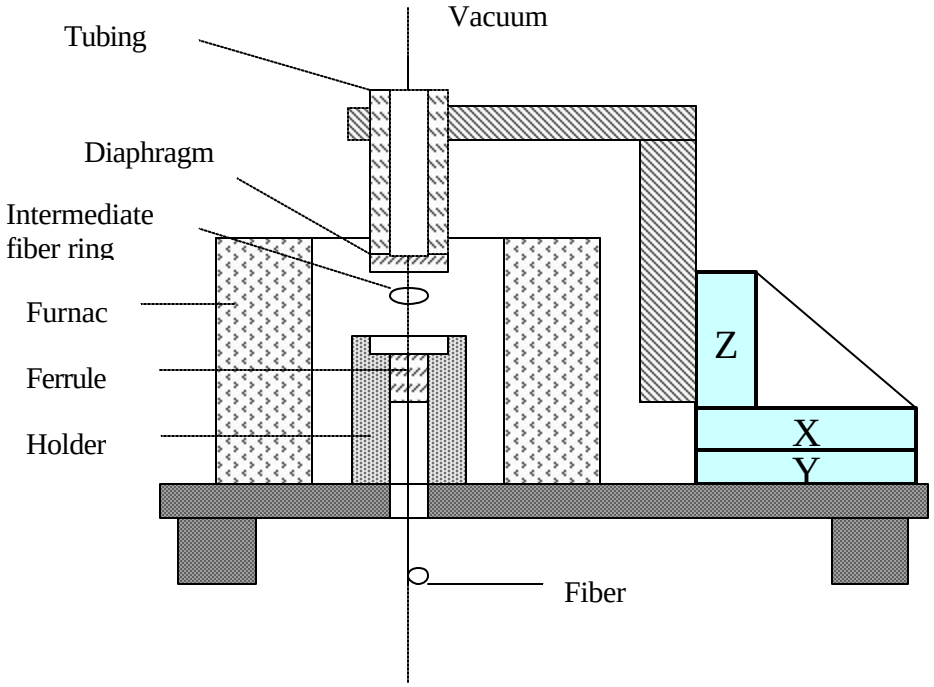

Figure 6.7. Acoustic sensor fabrication system using intermediate layer bonding method

7. High speed DSP-based signal processing techniques

In order to achieve the high frequency response for the measurement of acoustic signals or flow, high speed processing of the signals output by the SCIIB system will be necessary. Combining advanced digital signal processing (DSP) techniques with the novel SCIIB sensor will enable high speed on-line measurement of various high frequency signals with high accuracy. In this section of the report, we present our research work on the design and implementation of the advanced DSP-based signal processing techniques for the SCIIB sensor system.

7.1 DSP based SCIIB sensor system configuration

The configuration of the DSP-based high speed SCIIB sensor system is shown in Figure 7.1. The system includes an SCIIB sensor optical system, a DSP development platform, and an analog daughter module with A/D and D/A converters. Two important features are unique in this system. First, the output signals from the two channels of the SCIIB system are processed in the digital domain using a DSP chip. Second, in order to improve the system signal-to-noise ratio (SNR), the

light source is modulated at a high frequency, and synchronously demodulated at the receiving end. These two features enable low noise detection and demodulation of the weak optical signal at a very high speed.

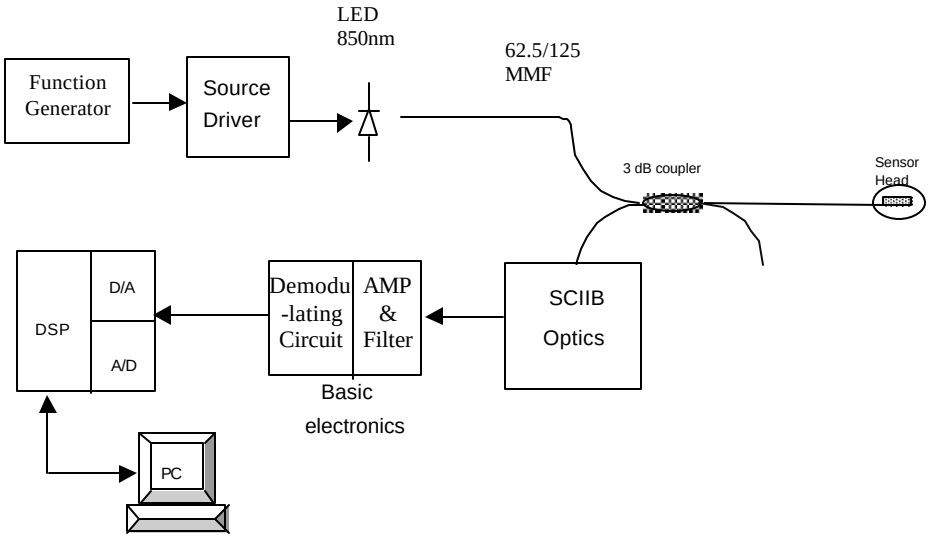

Figure 7.1. DSP based SCIIB high speed sensor system

7.2 System design and implementation

A prototype multimode DSP-based SCIIB system is currently under development based on the schematic shown in Figure 7.1. A 2 MHz sweep function generator (TENMA, Inc.) is used to modulate an 850 nm high power fiber optic LED (HFE4854, Honeywell) through a laser diode driver (Newport Corp). The modulated LED light is coupled in to a 62.5/125 multimode 3-dB 2x2 fiber coupler. One output leg of the coupler is connected to a SCIIB fiber sensor head, and the other output is inserted into index matching gel to eliminate reflections from the fiber tip. The signal output from the sensor head is transmitted back to the SCIIB optical box through the same fiber coupler. The SCIIB optic box splits the input signal into a reference channel (without bandpass filter) and a signal channel (with bandpass filter). Two photodetectors are used to convert the two channel signals to electrical signals. The detected signals are amplified, filtered and demodulated by means of the basic electronics, then sampled by an A/D module (ADCA Corp.) and processed in the DSP platform.

7.2.1 Optimal modulation scheme for the LED

Since amplitude modulation is used in the system to improve the SNR, we need to find an optimum operating modulation scheme for the light source. In order to make sure the HFE4856 LED works in its linear region during the modulation, we conducted an experiment to plot the current-power (I-P) curve of the LED as shown in Figure 7.2. Based on this result, we chose the operating point at 50 mA, and the modulation region from 10 mA to 90 mA. The modulating frequency is chosen to be 100 kHz.

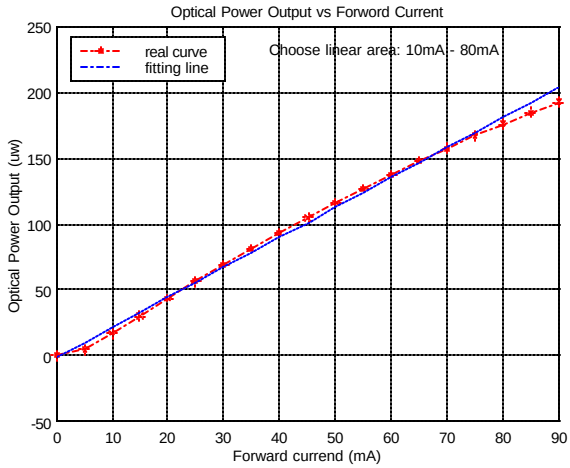

Figure 7.2. Current-power curve of the HEF4856 LED

7.2.2 Basic electronics design

The basic electronics involved in the system include the high frequency preamplifier circuit, the narrow bandpass filter circuit and the amplitude demodulation circuit. The specifications of the designed basic electronics include:

a) Modulation frequency: 100 kHz
b) Signal bandwidth: 10 kHz
c) Current gain for the reference channel: $x10^8$ A/V
d) Gain for the signal channel: $x10^9$ A/V
e) Signal-to-noise ratio: >60 dB

7.2.3 A/D converter design

An A/D converter is necessary to convert the amplified and demodulated signal to the digital domain so that the DSP hardware can further process the signal and improve the measurement accuracy.

To select the A/D module, we need to consider three factors: high accuracy, high throughput and ease of interface with the DSP hardeare. Through investigation of products from various of companies, we chose the DSP data acquisition board 5404DHR-V manufactured by ADAC, Inc. The 5404DHR-V board provides a 16-bit A/D with a maximum throughput of 100K samples/s, two 16-bit D/A voltage output channels, 8 multiplexed analog input channels and 4 C40 Comm ports to communicate with TM320C40 DSPchips.

7.2.4 DSP hardware design

TM320C4X series DSP chips made by Texas Instruments have successfully been used in various enginnering practices. The TMS320C40 is the original member of the 'C4x family. It features a power CPU that can deliver up to 30 MIPS/60 MFLOPS, 6 built-in communication ports allowing high speed data exchange, the capability of parallel processing by group several DSP chips together, and well-developed supporting software.

We selected the SMT320 DSP system manufactured by Sundance, Inc. as the main DSP development platform for the system. The platform consists of a SMT320 PCI carrier board with 4 TIM-40 module slots and a SMT302 TIM-40 module. The advantage of this structure is ease in extension to more C40s for parallel processing. The high-speed communication between the DSP platform and the A/D module is realized by using the Comm-ports of the DSP.

7.2.5 Software design

The development of the supporting software for the DSP system is the most critical part of the whole system design. The software will have a significant influence on the final system performances. The DSP supporting software is currently under preliminary development. It is based on the mixed programming of C language and the 3L DSP function library. The main functions of the DSP supporting software will include the data acquisition, data transferring, digital filtering, signal demodulation, and data output.

8. Plans for Year 2 Research

This section of the report presents plans for second year of the research program. The main objective for this three and one-half year program is the development and demonstration of cost-effective, reliable optical fiber sensors for the measurement of temperature, pressure, flow, and acoustic waves in downhole environments for use in oil recovery. The tasks proposed for the second year include continued development of the pressure and acoustic sensors, and initial designs and evaluation of the flow sensor. Improvement of the facility for automated fabrication of the SCIIB sensors will continue into the second year of the program. Extensive tests of the SCIIB sensors will be undertaken in the second year, in order to derive quantitative evaluations of the sensor resolution, accuracy, cross-sensitivity, repeatability and frequency response. In addition, the response of the fiber to overpressure conditions will be characterized. The sensors will be tested in water at elevated temperatures and pressures in order to assess the survival rate of the sensors in conditions representative of the downhole environment, and to appraise the protection afforded by various coatings that may be applied to the fiber. Commercially available coatings will be evaluated, and methods to provide hermetic protection to the fiber will be evaluated. Also, techniques for the multiplexing of multiple sensors along a single optical fiber will be investigated. The second year of the program will culminate in the testing of SCIIB sensors at the Department of Petroleum Engineering at the University of Tulsa, OK.

The estimated schedule for the proposed technical tasks during the second year research is presented in Figure 1. A detailed discussion of the tasks is given below.

8.1 Improvement and Evaluation of Sensor Fabrication

Development of methods and equipment for automated sensor fabrication will continue during the next year. The pressure sensor design will be tested and refined, if necessary, to accommodate possible overpressure to 20 kpsi. The beam delivery optics on the carbon dioxide laser used to fuse the fibers and capillary tube during assembly of the sensor probe will be modified to improve the uniformity of the sensor bonding, which is expected to improve optical performance as well as ensure seals that will withstand large hydrostatic loads. The sensor fabrication methods will be optimized by the application of Taguchi statistical process control methods to identify those manufacturing steps (and combinations of steps) that have the greatest impact on optical and mechanical performance of the sensors.

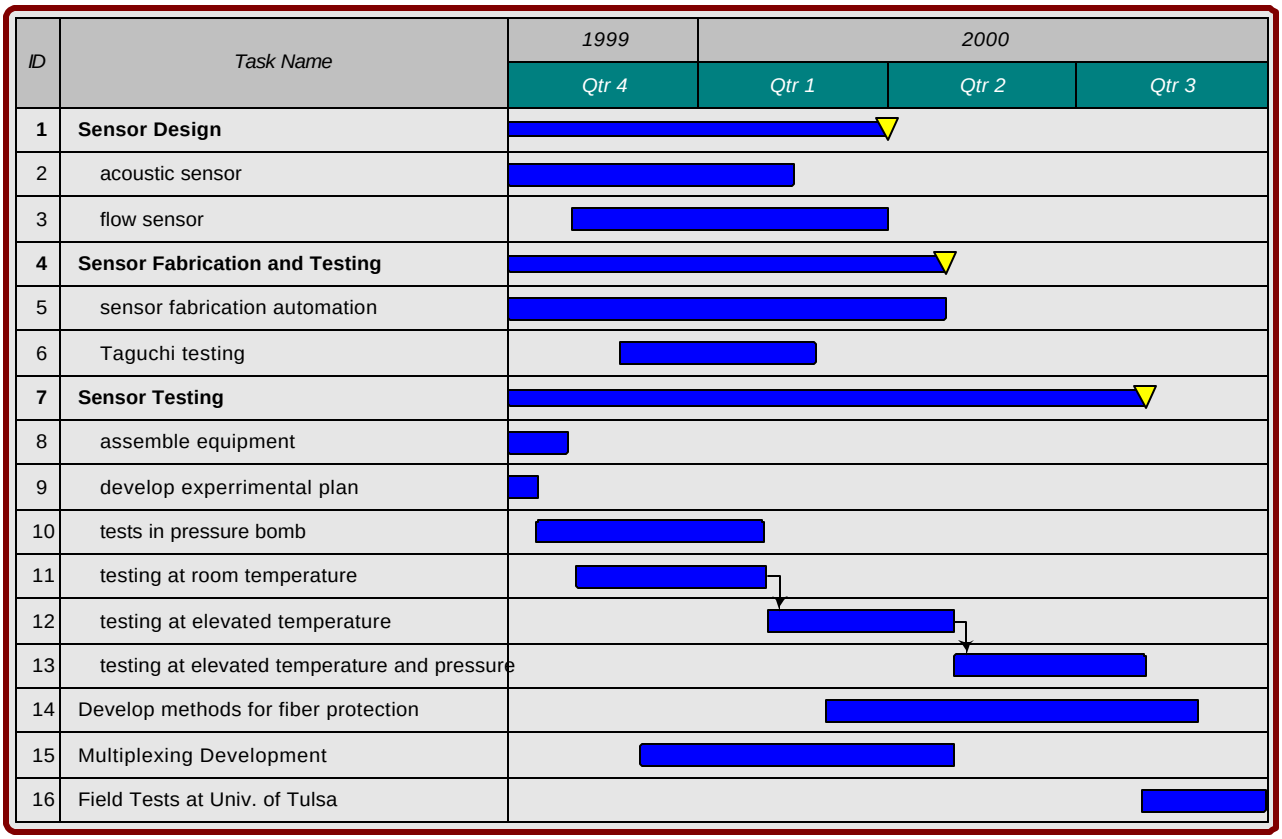

Figure 1. Estimated schedule for second year research

8.2 Acoustic Sensor Development

Acoustic (or seismic) signals are another very useful information in downhole oil recovery. The acoustic wave can generate very small pressures when it is propagating in the oil reservoir; therefore, the detection of the acoustic wave signals can be realized by pressure sensors with high sensitivity and high frequency response. For this task, we will continue with the development of acoustic sensor design and fabrication which was begun in the first year.

Since the SCIIB scheme has been proven to be effective for highly sensitive and accurate measurement of pressure, temperature, and acoustic waves, it is thus possible to design flowmeters based on the combination of the SCIIB sensor technology with various typical configurations, such as pitot tubes, orifices, thermal dispersion, acoustic dispersion and vortex shedding-induced vibration schemes. The ultra-small size of the SCIIB will allow the fabrication

of miniaturized flow sensors, which could be easily deployed in well boreholes, and would exert minimum perturbations in the measurement environment.

The first step of this task will be to investigate various flowmeter configurations and possible combinations of them with SCIIB sensors. Several best candidates will be chosen for further experimental testing and evaluation to determine the optimal sensor approach that can best meet the requirements for downhole instrumentation. Based on the chosen optimal sensor approach, complete sensors will then be designed and fabricated.

8.3 Sensor Test and Evaluation

Extensive tests of the SCIIB-based pressure, temperature, acoustic, and flow sensors will be undertaken during the second year. The objectives of these tests will be to assess the performance of the SCIIB sensors in terms of measurement accuracy, resolution, bandwidth, and repeatability, and to determine the robustness of the sensor and fiber optic cable in surviving the harsh downhole environment.

Using the pressure generators associated with the Pressure Systems Inc. pressure gauge calibrator and the Advanced Pressure Products calibrator, representative samples of the SCIIB sensors will be tested in water under high pressures and high temperatures for periods of up to two months at a time. Water is particularly significant for the proposed testing because it is present in the downhole environment, and promotes stress corrosion of the glass. The sensors will be characterized optically and mechanically before and after the long-term exposure to water. Optical tests will include measurement of spectral attenuation to determine if the exposure to water increased optical losses over any part of the near infrared spectrum. Mechanical tests will include determination of the fracture stress of the optical fiber. Surface analysis such as scanning electron microscopy, Raman spectroscopy, and FTIR spectroscopy may be used to determine if water has infiltrated into the glass network.

Sufficient tests of the sensors will be performed in order to generate a reasonable sample size to generate Weibull statistics with a high degree of confidence. Techniques for efficient experimental design, such as Taguchi methods, will be used to design the tests to optimize the experimental throughput. Efficient scheduling of tests will be required since some tests may last up to two months.

8.4 Development of Methods for Protection of Fiber

The downhole environment is expected to present conditions that may reduce the lifetime of unprotected optical fibers. Of greatest concern is catastrophic failure of the fiber due to stress corrosion fraction accelerated by exposure to water. Flaws in the surface of the glass produce sites with increased stress concentration. As the flaw grows due to stress concentration, water attacks the silica network, breaking the bonds that bridge the silicon and oxygen atom, and reducing the length of the silica macromolecules that give the fiber its tensile strength. In this process, the water disassociates into hydrogen and hydroxyl ions, which combine with the silicon and oxygen atoms of the glass to terminate the silica network:

$$\cdots\text{-O-Si-O-Si-O-Si-O} + 2H_2O \rightarrow \cdots\text{-O-Si-OH} + \text{HO-Si-O-}\cdots + H_2O$$

The disruption of the glass network weakens the glass, enabling further propagation of the flaw at the point of maximum stress concentration.

Clearly, a priority for this program must be development of methods to protect the fiber from stress corrosion which results from attack by water. According, during the next year, various commercial fibers with various coatings will be tested to assess the influence of the coating on the lifetime of the fiber. Fiber samples with epoxy acrylate, polyimide, or gold coatings will be placed in a pressure vessel with water and then sealed. The vessel will be heated at temperatures up to 200°C in order to generated pressurized steam, for period up to two weeks. The fibers will then be removed from the pressure vessel, and then examined under a microscope. They will then be subjected to a bend test to assess the strength of the fiber. In this test, a fixture will be used to bend the fiber in a decreasing bend radius until the fiber breaks. The radius at which the fiber fractures depends upon the strength of the fiber. Therefore, the minimum bend radius can be used to determine the fiber strength after exposure to the superheated steam.

8.5 Development of Sensor Multiplexing

Multiplexing of several sensors on a single optical fiber is highly desirable in many downhole applications to obtain real-time monitoring at multiple locations, which would allow the monitoring of wells and reservoirs over a large physical scale. More importantly, the capability

could also create new opportunities in multilateral well applications where multiple branch wells are drilled from a single main bore. The branch wells can be instrumented with multiplexed fiber sensors to monitor the entire branches, to determine pressure of the hydrocarbon producing geological zones, and flow to determine the amount of fluids and gas flowing from the lateral into the main bore. Sensor multiplexing is therefore important to the oil industry.

One of the most significant advantages of fiber sensor technology is the capability of multiplexing of a large number of sensor elements in a single system, resulting from the tremendous bandwidth offered by optical fiber, which has been largely exploited in communications. This task will be to develop optimal schemes for the multiplexing of the sensors designed in the preceding task.

Typical methods for fiber sensor multiplexing include wavelength division multiplexing (WDM), optical time domain reflectometry (OTDR), coherence multiplexing (CM), and code division multiple access (CDMA), and combinations of some of these methods. In this task, these methods and their variations will be investigated in detail. Emphasis will be placed on the determination of maximum number of multiplexed sensor elements, the relation between power throughput and sensor signal-to-noise ratio, crosstalk between sensor elements, and the complexity of sensor interrogation. Optimal architectures that can best support the multiplexing of the sensors will be developed to support the sensor instrumentation system.

8.6 Field Tests at University of Tulsa

This task will be to systematically test the instrumentation systems developed at Virginia Tech in the field laboratory in the Department of Petroleum Engineering at the University of Tulsa, OK, where extensive specialized facilities and operation systems are available to support the sensor in-house testing. A High-Temperature High-Pressure (HTHP) test loop, will provide the widest range of applications for testing all of the fiber sensor instrumentation developed by Virginia Tech. The HTHP Loop will allow sensor testing to be conducted through pipe-wall penetrations in order to measure pressure, temperature, flow, and acoustic waves in single as well as two and three phase flow. Pipe diameters which will be made available are 2-inch up to 8-inch. Through special connections, testing in simulated down-hole conditions will also be possible. Testing conditions will range in pressures from inches of water column to 2200 psig and temperatures from 40 °F to 200 °F. Flow rates will generally vary from 0.5 to 5 feet per second.

9. Conclusions

This report presents the detailed research work and technical progress from October 1, 1998 to September 31, 1999. The research work in this reporting period was concentrated on specifying the technical requirements, on the design and fabrication of various fiber optic sensor probes, on the design and implementation of SCIIB sensor systems, and on the development of DSP-based signal processing techniques.

The research work and the corresponding conclusions are summarized as below.

1) Specification of technical requirements

The technical requirements for the real time measurement and monitoring of the key parameters involved in downhole applications have been specified by working closely with the scientists and engineers from Chevron Research and Technology Company and Baker Hughes. These specifications cover the measurements of temperature, pressure, and flow for downhole applications, and have been used as guidelines in the sensor design and fabrication.

2) Development of the automated SCIIB sensor fabrication system

An automated SCIIB sensor fabrication system was successfully developed to allow the fabrication of high quality SCIIB sensors. The system includes the CO_2 laser heating subsystem, the white light air gap monitoring subsystem, and the computer controlled ultra-precision micro-positioning subsystem. The CO_2 laser, used as the heating source for bonding the glass tube and fibers together, is controlled by a host computer so that its power level and exposure duration are optimized for the sensor fabrication. The air gap length of the SCIIB sensor is monitored by the white light subsystem with an accuracy of a few nanometers. The computer controlled micro-motion system precisely positions the fibers and tube to allow an accurate adjustment of the length of the air gap and the effective gauge length of the sensor. These three subsystems are coordinated through a sophisticated control program to achieve an optimal operation of the whole system. Extensive experiments and tests have been conducted to find the best parameters for fabricating high quality SCIIB sensors.

With the help of the automated sensor fabrication system, multimode and single-mode fiber SCIIB sensor probes can now be made in larger quantity to satisfy the immediate needs for further comprehensive tests and evaluations of the SCIIB sensors and systems.

3) SCIIB pressure sensor probe design and fabrication

SCIIB pressure sensors were designed to cover the pressure ranges of interest. Using the automated sensor fabrication system, a large number of high-quality SCIIB pressure sensors were successfully fabricated. These pressure sensors had their initial air gaps and effective gauge lengths optimized for very low cross-sensitivity to temperature.

To evaluate those pressure sensors, two pressure testing system were designed. The first system was designed based on the Model 9035 pressure calibrator purchased from Pressure Systems, Inc. This system can generate pressure up to 200 psia, and will allow us to test sensor performance with an accuracy of 0.5 psia. The second system was a 20,000 psia pressure calibration system based on the APCS controller and generator manufactured by Advanced Pressure Products, Inc., which will allow us to test accuracy, repeatability, and hysteresis of the SCIIB sensors under high pressures at elevated temperatures.

4) SCIIB temperature sensor probe design and fabrication

A larger number of SCIIB temperature sensors have been designed, fabricated, and tested. The tests include the evaluation of the sensor survivability and thermal stability, the measurement of differential coefficient of thermal expansion (ΔCTE), and the standard deviation. The test results indicate that the sensor probes satisfy all the specifications required for the downhole applications.

5) Acoustic sensor design and implementation

Thin silica diaphragm-based fiber optic acoustic sensors were designed to detect the seismic signals for downhole applications. Detailed analyses were performed to achieve the optimal design of the frequency response and the resolution for detection of acoustic signals. Various bonding techniques were studied to fabricate the acoustic sensor, among which controlled thermal bonding technologies were investigated intensively. Encouraging progress has been made in bonding the thin silica diaphragm to the silica tube through a direct bonding method and an intermediate layer method. Further research work is necessary to improve the sensor fabrication techniques to make high performance acoustic sensors.

6) Development of high-speed DSP-based signal processing

Advanced DSP-based signal processing techniques were designed to achieve high-speed detection of the acoustic or flow signals for downhole applications. A prototype DSP-based

SCIIB sensor system was implemented. The system utilized an amplitude modulation scheme to allow high frequency detection of weak optical signals with a high signal-to-noise ratio. Further research will be concentrated on software development and system optimization.

7) Development of SCIIB sensor systems

Two SCIIB sensor systems have been successfully designed, fabricated and tested. The multimode fiber based SCIIB sensor system was designed for short distance applications at low cost, and the single-mode fiber based SCIIB sensor system was optimized for long distance applications. Test results indicate that the SCIIB systems possess the advantages of both intensity-based and interferometric fiber optic sensors, and have the capability of self-compensation for the drifting of the source power and the fluctuation of fiber attenuation. The test results obtained from the single-mode fiber SCIIB sensor system also suggest that bend insensitive fibers be used to minimize the measurement error induced by the changes in the spectrum propagating through the optical fibers.

The research performed over the first ten months of the program has followed the schedule as proposed, and solid research progress has been made in design and fabrication of the SCIIB sensor probes, development of the sensor systems, and construction of the test systems. These technical achievements will significantly help to advance continued research on sensor tests and evaluation during the second year of the program.

10. References

1. B. B. Muvdi, J. W. McNabb, “Engineering Mechanics Materials”, pp597-602 ,Macmillian Publishing Company, 1984,

2. E. J. Hearn, “Mechanics of Materials”, pp194-217, Pergamon Press, 1977.

3. Mario Di Giovanni, “Flat and Corrugated Diaphragm Design Handbook”, (New York: MArcel Dekker), 1982.